Cell Reports
Medicine

Article

Multiplex immune profiling reveals the role of serum immune proteomics in predicting response to preoperative chemotherapy of gastric cancer

Graphical abstract

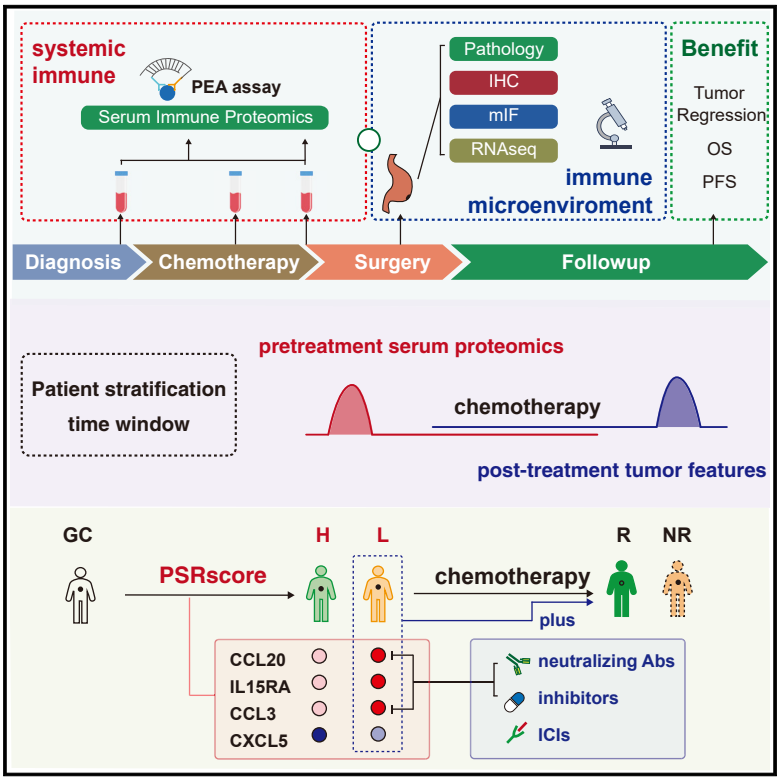

Highlights

- Both local and systemic immune features are associated with chemotherapy response
- Pretreatment serum immune proteomics can stratify patients
- A pretreatment serum protein scoring system is established for response prediction

Authors

Zhaoqing Tang, Yuan Gu, Zhongyi Shi, ..., Yuehong Cui, Yihong Sun, Xuefei Wang

Correspondence

cui.yuehong@zs-hospital.sh.cn (Y.C.),
sun.yihong@zs-hospital.sh.cn (Y.S.),
wang.xuefei@zs-hospital.sh.cn (X.W.)

In brief

Responses toward preoperative chemotherapy are heterogeneous in patients with gastric adenocarcinoma. Tang et al. report that both local and systemic immune features are involved in the treatment response of preoperative chemotherapy. They also establish a pretreatment serum protein scoring system for response prediction and patient stratification.

Tang et al., 2023, Cell Reports Medicine *4*, 100931
February 21, 2023
https://doi.org/10.1016/j.xcrm.2023.100931

CellPress

Cell Reports Medicine

CellPress
OPEN ACCESS

Article

Multiplex immune profiling reveals the role of serum immune proteomics in predicting response to preoperative chemotherapy of gastric cancer

Zhaoqing Tang,[1,2,3,6] Yuan Gu,[1,6] Zhongyi Shi,[1,6] Lingqiang Min,[1] Ziwei Zhang,[1] Peng Zhou,[1] Rongkui Luo,[4] Yan Wang,[5] Yuehong Cui,[5,*] Yihong Sun,[1,2,*] and Xuefei Wang[1,2,3,7,*]

[1]Department of General Surgery, Zhongshan Hospital, Fudan University, Shanghai 200032, China
[2]Gastric Cancer Center, Zhongshan Hospital, Fudan University, Shanghai 200032, China
[3]Department of General Surgery, Zhongshan Hospital (Xiamen), Fudan University, Shanghai 200032, China
[4]Department of Pathology, Zhongshan Hospital, Fudan University, Shanghai 200032, China
[5]Department of Medical Oncology, Zhongshan Hospital, Fudan University, Shanghai 200032, China
[6]These authors contributed equally
[7]Lead contact
*Correspondence: cui.yuehong@zs-hospital.sh.cn (Y.C.), sun.yihong@zs-hospital.sh.cn (Y.S.), wang.xuefei@zs-hospital.sh.cn (X.W.)
https://doi.org/10.1016/j.xcrm.2023.100931

SUMMARY

Responses toward preoperative chemotherapy are heterogeneous in patients with gastric adenocarcinoma. Existing studies in the field focus heavily on the tumor microenvironment (TME), whereas little is known about the relationship between systemic immunity and chemotherapy response. In this study, we collect serum samples from patients with gastric adenocarcinoma before, on, and after preoperative chemotherapy and study their immune proteomics using an antibody-based proteomics panel. We also collect surgically resected tumor samples and incorporate multiple methods to assess their TME. We find that both local and systemic immune features are associated with treatment response. Preoperative chemotherapy induces a sophisticated systemic immune response indicated by dynamic serum immune proteomics. A pretreatment serum protein scoring system is established for response prediction. Together, these findings highlight the fundamental but largely underestimated role of systemic immunity in the treatment of gastric cancer, suggesting a patient stratification strategy based on pretreatment serum immune proteomics.

INTRODUCTION

Gastric cancer, of which gastric adenocarcinoma (GAC) is the major histological type, is one of the most common malignancies and major causes of cancer-related mortalities worldwide.[1,2] A considerable proportion of patients with gastric cancer are diagnosed in the advanced stage, which largely limits treatment efficacy and patient prognosis.[3] With surgical resection still being the mandatory backbone in treatment, several studies, including JCOG9501 and JCOG9502, have shown that patients with gastric cancer would not benefit from extended resection.[4–6] In the last decade, neoadjuvant and perioperative treatments have brought new hope. The MAGIC trial showed that three preoperative and three post-operative cycles of ECF (epirubicin, cisplatin, and 5-fluorouracil) chemotherapy improved the 5-year survival rate from 23% to 36% for patients with resectable stage II/III gastric cancers compared with surgery alone.[7] The FLOT4-AIO trial further showed that FLOT (5-fluorouracil, folinic acid, oxaliplatin, and docetaxel) regimen led to better pathological response rates, R0 resection rates, and overall survival (OS) compared with ECF or ECX (epirubicin, 5-fluorouracil, and capecitabine).[8,9] It is recognized that preoperative treatment with chemotherapy could increase the chance for curative resection, eliminate early microscopic spread, and allow a preoperative response assessment of adjuvant treatment.[10] With new drugs such as immune checkpoint inhibitors (ICIs) emerging, chemotherapy remains the most fundamental and accessible component in the perioperative treatment of gastric cancer.

On the other hand, preoperative treatment in gastric cancer is still controversial, especially in east Asian countries. The responses toward preoperative chemotherapy are heterogeneous, while the knowledge of its mechanism is limited.[11] Biomarkers that predict patient response toward preoperative chemotherapy are needed to stratify patients for optimal treatment. Emerging evidence has shown that immunity is involved in patient response to chemotherapy. Choi et al. reported that stromal programmed cell death ligand 1 (PD-L1) expression in tumor specimens predicted the benefit from adjuvant chemotherapy after D2 gastrectomy for stage II/III gastric cancer.[12] Kim et al. used paired pretreatment and on-treatment gastric biopsy samples during standard first-line chemotherapy and identified chemotherapy-induced natural killer (NK) cell infiltration, macrophage repolarization, and increased antigen presentation among treatment responders.[13] However, existing studies in the field of gastric cancer immunology have focused heavily on local immune responses in the tumor microenvironment (TME), and little

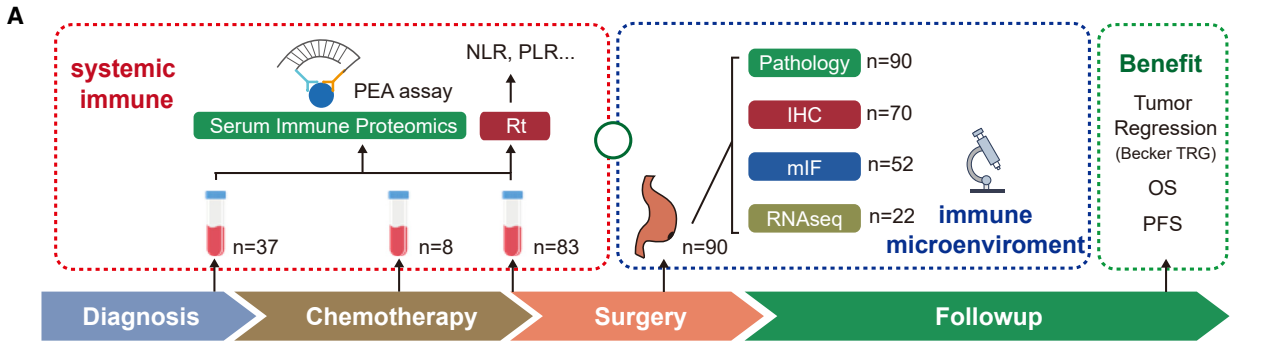

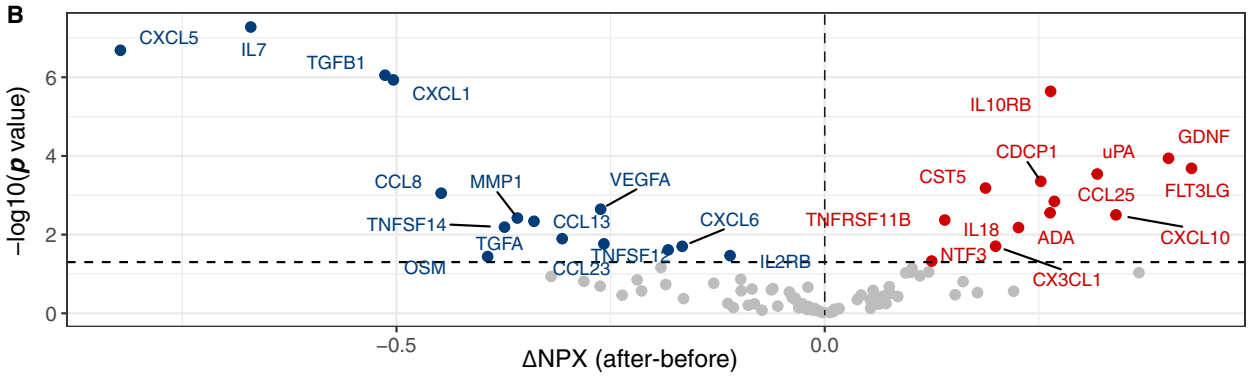

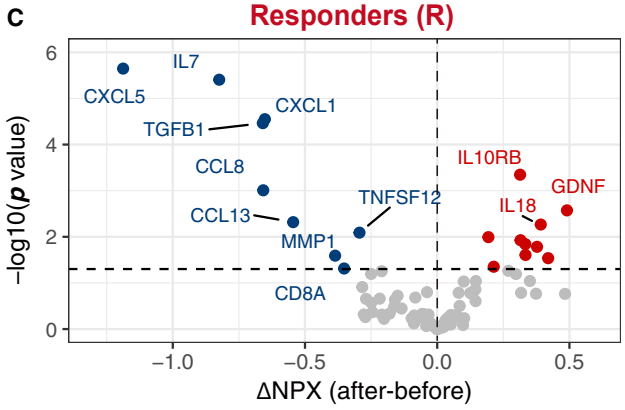

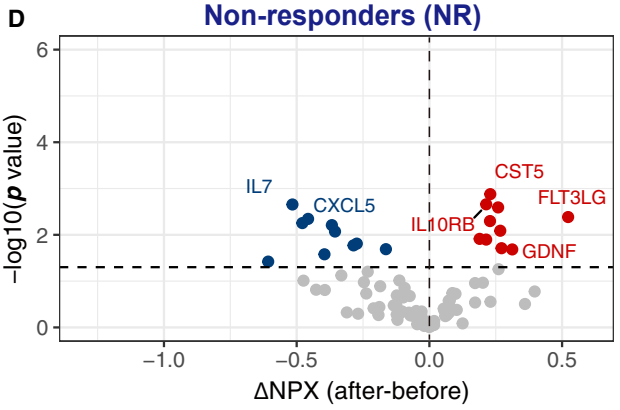

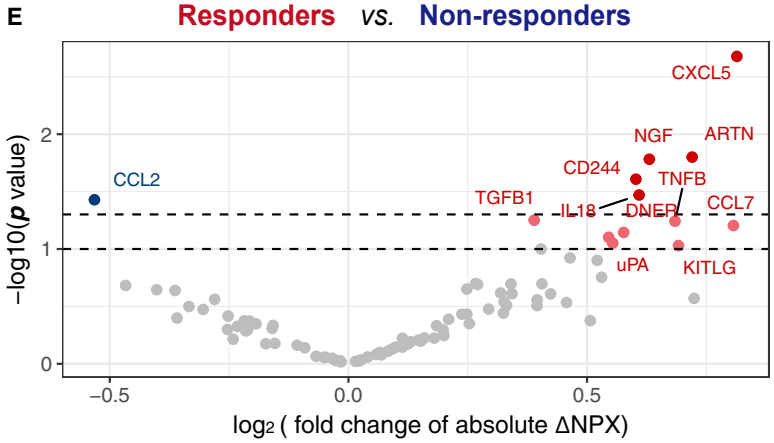

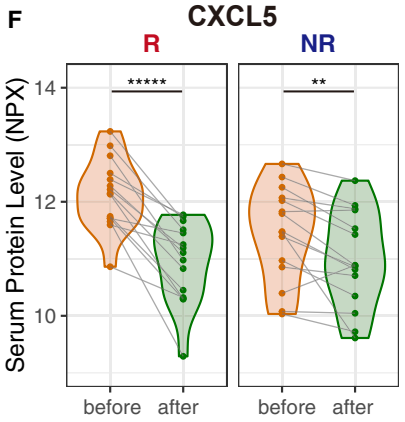

(legend on next page)

is known about the relationship between systemic immunity and chemotherapy response in gastric cancer.

Gastric cancer is a systemic disease. Immunity stimulated by tumor burden and antitumor treatment is coordinated across different tissues. Profiling the systemic immune landscape or immune macroenvironment as described by Hiam-Galvez et al.[14] of patients receiving preoperative chemotherapy is important for the complete understanding of cancer immunity and mechanism of treatment resistance. Existing systemic immune-inflammation indices such as the neutrophil-to-lymphocyte ratio (NLR) are mostly dependent on blood cell counts, which limit their dimensions.[15–17] Serum immune proteomics, with its high content, would be an ideal reflection of systemic immunity.[18–22] In this study, we collected serum samples from patients with GAC before, on, and after preoperative chemotherapy and studied their immune proteomics using an antibody-based proteomic platform (Olink Target 96 Inflammation panel). We also collected surgically resected tumor samples from these patients and incorporated multiplex immunofluorescence (mIF), immunohistochemistry (IHC), and RNA sequencing (RNA-seq) to assess the TME. Dynamics of serum immune proteomics and their correlations with the TME were studied. Biomarkers were identified to predict tumor regression, OS, and progression-free survival (PFS) of patients receiving preoperative chemotherapy.

RESULTS

Study population

Ninety patients with GAC receiving preoperative chemotherapy and following gastrectomy were included in this study (Figure 1A). Patients were excluded if they received ICIs during preoperative periods. Eligible patients were divided into responders (residual tumor/tumor bed $\leq$50% with chemotherapy effect, Becker TRG score 1–2) and non-responders (Becker TRG score 3). Of 90 patients, 36 (40%) achieved a tumor regression score of 1–2 and were regarded as responders. Patients with better tumor regression had a significantly longer OS compared with non-responders (Figure S1A). PFS showed a similar trend, though with no statistical differences (Figure S1B). The basic clinical characteristics of the patients are summarized in Table S1. Nearly half of the patients received two-drug cytotoxic chemotherapy, most of which were SOX (S-1 plus oxaliplatin) or XELOX (capecitabine plus oxaliplatin) regimens. The rest of the patients received three-drug cytotoxic chemotherapy, which was primarily a DOS (docetaxel, oxaliplatin, and S-1) regimen. By the date of analysis on March 1, 2022, the median follow-up time was 55.8 months (range from 3.2 to 82.7 months). In the overall population, the median PFS was 39.8 months (95% confidence interval [CI], 32.7 to not reached [NR]), whereas the median OS was 63.9 months (95% CI, 51.8 to 74.1), with 45 mortalities (50%).

Dynamics of serum immune proteomics are associated with the response to preoperative chemotherapy

Thirty-seven pretreatment, eight on-treatment, and 83 post-treatment serum samples from patients receiving preoperative chemotherapy were collected, among which 30 pretreatment and 30 post-treatment serum samples were paired (Figure 1A). Levels of 92 marker proteins in key immune and inflammation pathways were measured by proximity extension assay (PEA) using Olink Target 96 Inflammation panel. Comparison of protein levels in pre- and post-treatment serum samples showed the dynamics of serum immune proteomics after preoperative chemotherapy. Eighteen of 92 proteins showed a significant change in both paired and unpaired tests (Figures 1B, S1C, and S1D), indicating sophisticated systemic immune responses induced by preoperative chemotherapy. Among them, serum C-X-C motif chemokine ligand 1 (CXCL1) and CXCL5 levels showed a significant decrease after preoperative chemotherapy (Figure S1D). Interestingly, Zhou et al. reported that CXCL1 and CXCL5 as CXCR2 ligands could significantly promote migration of gastric cancer cells and drive gastric cancer metastasis.[24] Downregulation of serum CXCL5 and CXCL1 by chemotherapy may help prevent gastric cancer metastasis. Indeed, CXCL1/5 levels decreased in the early cycles of preoperative chemotherapy (Figure S1E).

We further compared the dynamics of serum immune proteomics in patients with different treatment responses. We found that the responders showed a more dynamic change of serum immune proteomics after treatment (Figures 1C and 1D). We also compared the absolute change of protein levels after chemotherapy between the responders and non-responders and found that immune protein levels showed overall larger changes after chemotherapy in the responders (Figure 1E). For example, the decrease of serum CXCL5 level after treatment was much milder in the non-responders compared with the responders (Figures 1C–1F). On-treatment proteomics also seemed to differ in responders and non-responders (Figure S1E). For example, serum interleukin receptor subunit β (IL-10RB) and IL-18 levels tended to increase during chemotherapies in responders but not in non-responders (Figures S1F and S1G), though conclusions of this part could be limited by sample numbers.

Together, these results showed sophisticated systemic immune responses toward preoperative chemotherapy in patients

Figure 1. Dynamics of serum immune proteomics are associated with response to preoperative chemotherapy

(A) Flow chart of sample collection and study design.

(B) Volcano plot showing serum proteins whose levels changed after preoperative chemotherapy by paired tests (n = 30 pairs).

(C) Volcano plot showing serum proteins whose levels changed after preoperative chemotherapy by paired tests in the responders (N = 15).

(D) Volcano plot showing serum proteins whose levels changed after preoperative chemotherapy by paired tests in the non-responders (N= 15).

(E) Volcano plot showing serum proteins whose absolute level changes after preoperative chemotherapy differed between the responders and non-responders (responder N= 15; non-responder N = 15).

(F) Change in serum protein level of CXCL5 after preoperative chemotherapy in patients with different treatment responses (responder N = 15; non-responder N = 15).

(*p < 0.05, **p < 0.01, ***p < 0.001, ****p < 0.0001; ns, not significant; n = 3; t test).

See also Figure S1.

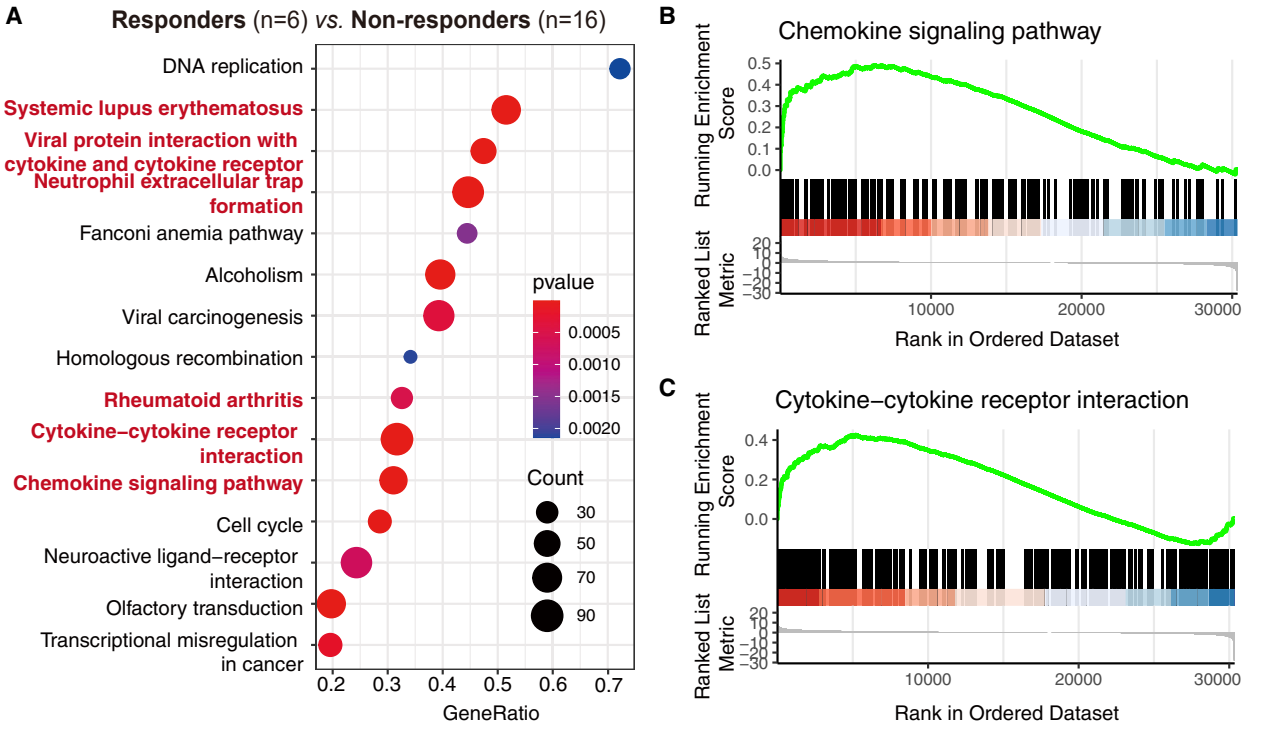

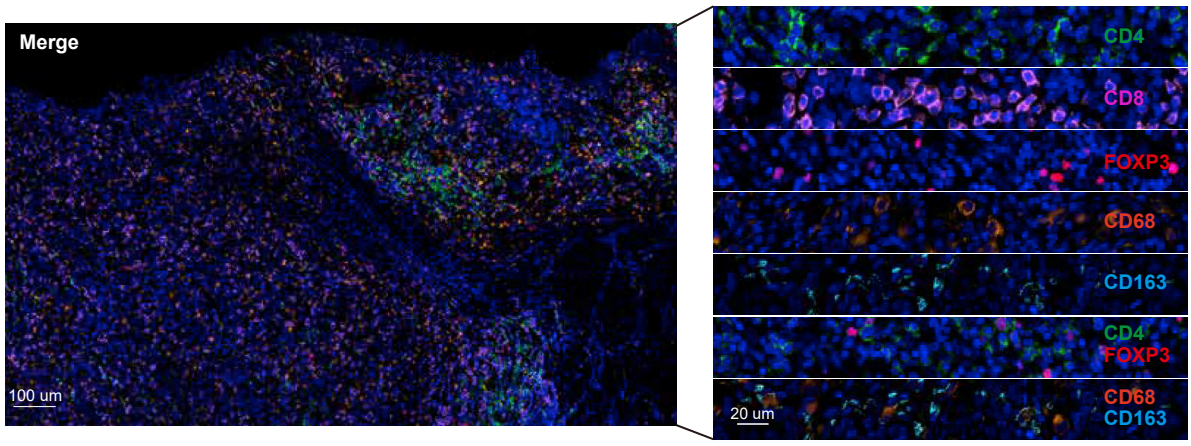

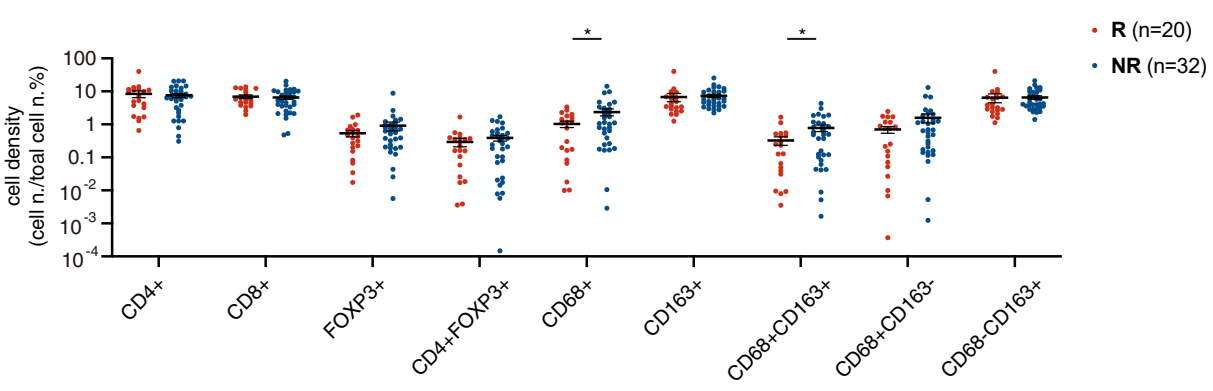

(legend on next page)

with GAC. The responders tended to have more dynamic systemic immune responses after preoperative chemotherapy.

TME is associated with patient response to preoperative chemotherapy

We first compared the transcriptomes of tumor samples from patients with different treatment responses in order to acquire a general knowledge of tumor local features. Gene set enrichment analysis (GSEA) showed the hallmark pathways altered in the good responders (Figure 2A). Alteration of pathways like DNA replication and cell cycle may indicate suppression of cancer cell proliferation and regression of tumors. Apart from that, nearly half of the pathways were associated with immunity, such as the chemokine signaling pathway and the cytokine-cytokine receptor interaction pathway (Figures 2B and 2C), indicating the importance of immunity in chemotherapy.

We therefore evaluated the geographical immune landscape in surgically resected tumor samples by mIF. CD4, CD8, and Foxp3 staining was used to identify different types of T cells. CD68 and CD163 staining was used to identify macrophages (Figure 2D). We compared immune infiltration between responders and non-responders. The cell densities of $CD68^+$ macrophages and $CD68^+/CD163^+$ M2 macrophages were significantly higher in non-responders (Figures 2E and S2A). Correspondingly, Xing et al. reported higher $CD68^+$ macrophages infiltration in non-responders with gastric cancer after neoadjuvant chemotherapy.[24] M2 macrophage was also shown to be involved in chemoresistance in various types of cancers.[25–29]

Meanwhile, we collected 24 pretreatment endoscopic biopsy samples from patients in the cohort. mIF was used to profile the pretreatment TME (Figure S2B). Notably, most endoscopic biopsies only got superficial mucosa of stomach, which largely limited their representativeness of the whole tumors and comparability to surgically resected tissues (Figure S2C). Indeed, mIF showed that immune cell infiltration in pretreatment TME had no differences between the responders and non-responders (revised Figure S2D), which could be a result of the limited biopsy depth and significant intratumoral heterogeneity of gastric cancer.

Together, these results showed that post-treatment TME was associated with response to preoperative chemotherapy.

Correlations between serum immune proteomics and TME

Given that most existing studies of cancer immunology focused on the TME, we evaluated the correlations between systemic immunity and the TME. We also determined the correlation between serum immune proteomics and immune cell infiltration in the TME. Interestingly, the post-treatment TME seemed to be more related to pretreatment than post-treatment serum immune proteomics. Correlations between pretreatment serum immune proteomics and immune cell infiltration were overall stronger even with smaller sample numbers (Figures 3A and 3B). For instance, higher pretreatment serum fibroblast growth factor 21 (FGF21) level was correlated with less infiltration of $CD68^+$ macrophages, while a higher pretreatment serum transforming growth factor β1 (TGF-β1) level was correlated with more infiltration of $CD4^+$ T cells (Figures 3C and 3D). In fact, TGF-β was reported to have pleiotropic effects on the regulation of effector and regulatory CD4-positive cell responses.[30] Correlations between post-treatment serum immune proteomics and post-treatment immune cell infiltration were also observed. For instance, a higher pretreatment serum C-C motif chemokine ligand 11 (CCL11) level was correlated with more infiltration of $CD4^+/FOXP3^+$ T cells (Figure 3E). Wang et al. reported that CCL11 increased the proportion of $CD4^+CD25^+Foxp3^+$ regulatory T cells (Tregs) in breast cancer.[31] More work is needed to explore whether CCL11 regulates $CD4^+Foxp3^+$Treg cell function in gastric cancer.

We also evaluated the correlations between post-treatment serum protein level and tumor mRNA level of the 92 immune genes. Five of the 92 correlations showed statistical significance, with only two positive, as expected (Figures 3F and S3A–S3E). The correlation strength of TNFSF12 and CCL4 was actually marginal (Figures S3A and S3B). The correlations between the serum protein levels and tissue gene mRNA levels were overall weak.

These results showed the communications and interdependency between systemic immunity and the TME. Research on the TME cannot fully reveal how the immune system responds to gastric cancer and antitumor treatment as a whole. More efforts should be devoted to profiling systemic immunity in patients with gastric cancer.

The clinical values of classic systemic immune-inflammation indices

Classic systemic immune-inflammation indices were mostly based on blood cell ratios and were proven to be linked to patients' clinical outcomes.[16] We were curious about the connections between serum immune proteomics and classic systemic immune-inflammation indices. Thus, we evaluated the correlation between post-treatment serum immune proteomics and classic immune-inflammation indices, including the NLR, the platelet-to-lymphocyte ratio (PLR), the monocyte-to-lymphocyte ratio (MLR), and the platelet distribution width (PDW) as well as common blood cell counts. While most correlations were relatively weak (Figure S3F), serum CXCL5 and CXCL1 levels showed a strong correlation with platelet count (Figures S3G and S3H). With CXCL1 and CXCL5 are usually involved in the homeostasis

Figure 2. TME is associated with response to preoperative chemotherapy

(A) GSEA showing the pathways altered in the tumors of responders (responder n = 6; non-responder n = 16). Immune-related pathways are marked in red.

(B) Enrichment plot of chemokine signaling pathway.

(C) Enrichment plot of cytokine-cytokine receptor interaction pathway.

(D) Representative images of multiplex immunofluorescence. Colors of the staining of different protein markers are indicated.

(E) Comparison of immune cell infiltration in post-treatment tumor samples from patients with different treatment responses (responder n = 20; non-responder n = 32). Cell density calculated by positive cell numbers/total cell numbers. Data are represented as the mean ± SEM (*$p < 0.05$; t test).

See also Figure S2.

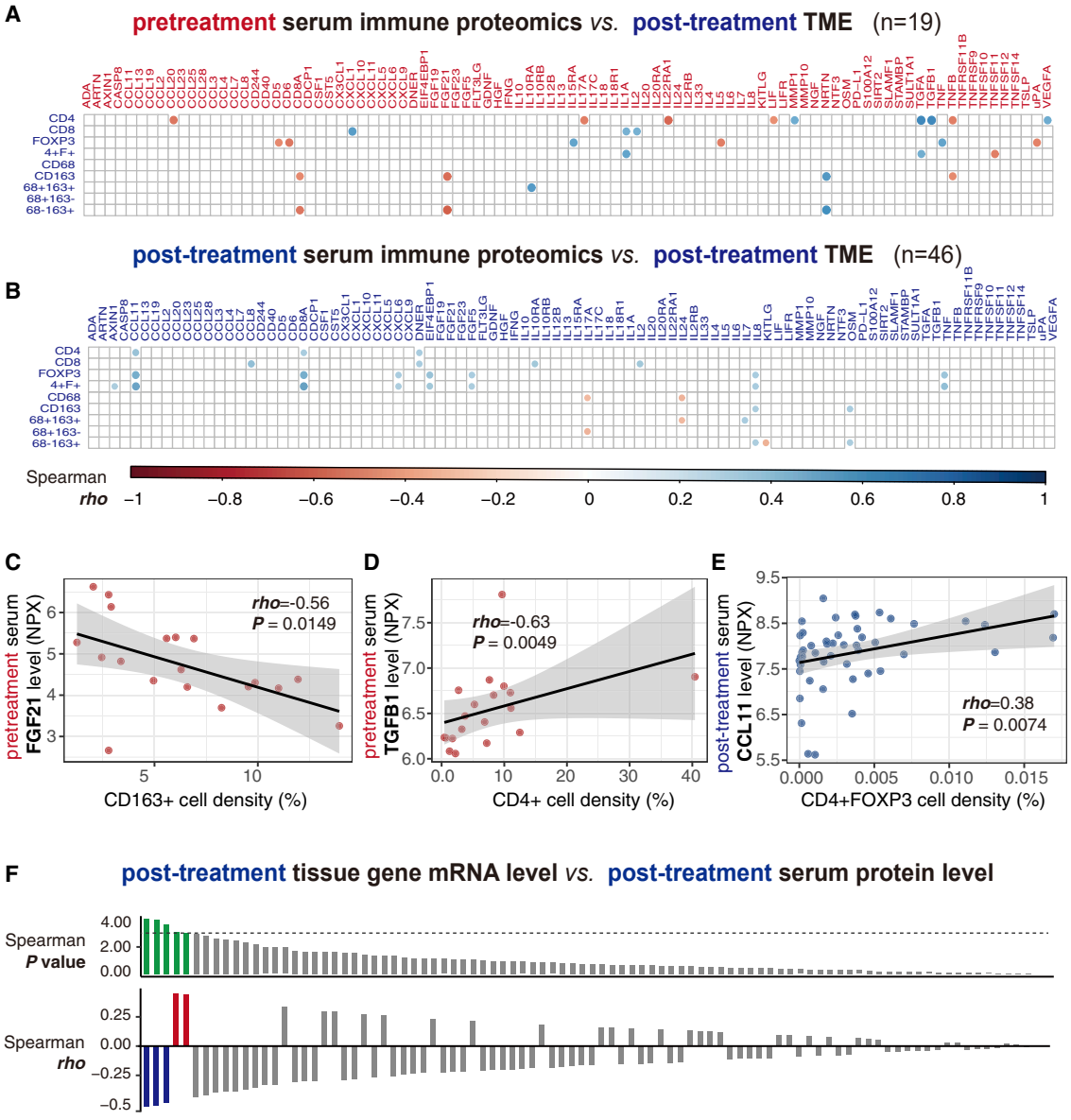

Figure 3. Correlations between serum immune proteomics and TME

(A) Correlations between pretreatment serum immune proteomics and post-treatment immune cell infiltration in TME. The rho values of correlations with p <0.05 are indicated by different colors, n = 19.

(B) Correlations between post-treatment serum immune proteomics and post-treatment immune cell infiltration in TME. The rho values of correlations with p <0.05 are indicated by different colors, n = 46.

(C) Correlation between pretreatment serum FGF21 level and post-treatment $CD163^+$ cell infiltration in TME.

(D) Correlation between pretreatment serum TGFB1 level and post-treatment $CD4^+$ cell infiltration in TME.

(E) Correlation between post-treatment serum CCL11 level and post-treatment $CD4^+FXOP3^+$ cell infiltration in TME. The rho and p values of Spearman's correlation as indicated.

(F) The p and rho values of Spearman's correlation between tissue gene mRNA level and serum protein level of 92 proteins. n = 22 paired samples. Proteins with p <0.05 are marked in green. Proteins with positive correlation are marked in red. Proteins with negative correlation are marked in blue.

See also Figure S3.

and function of neutrophil,[15,32,33] more work is needed to understand this unexpected but interesting correlation. We also evaluated the correlation between classic systemic immune-inflammation indices and TME features. No correlations were observed between post-treatment classic immune-inflammation indices and immune cell infiltration in the TME (Figure S3I).

We further explored the clinical values of classic systemic immune-inflammation indices and evaluated the treatment

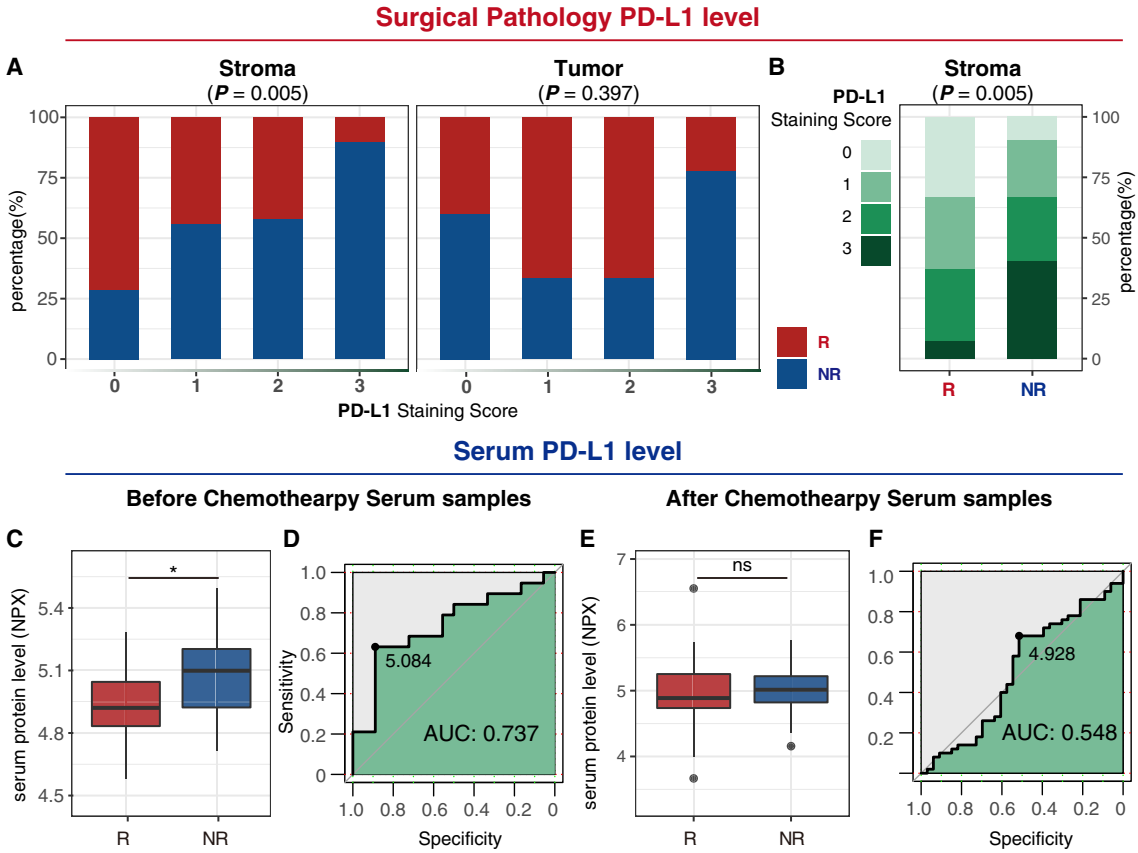

Figure 4. Post-treatment tumor stromal PD-L1 level and pretreatment serum PD-L1 level both predict preoperative chemotherapy response

(A) Treatment response in patients (N = 70) with different stromal/tumor PD-L1 staining scores. p value was calculated by chi-squared test.

(B) Stromal PD-L1 staining scores of patients with different treatment responses. p value was calculated by chi-squared test.

(C) Responders (N = 18) had lower serum PD-L1 level before treatment compared with non-responders (N = 19).

(D) ROC curve demonstrating the treatment response predictive accuracy of pretreatment serum PD-L1 level.

(E) Post-treatment serum PD-L1 level showed no difference between responders (N = 18) and non-responders (N = 19).

(F) ROC curve demonstrated the treatment response predictive accuracy of post-treatment serum PD-L1 level.

See also Figure S4.

response predictive values of NLR, PLR, MLR, and PDW. Receiver operating characteristic (ROC) curves of the four indices were drawn with the highest area under the curve (AUC) of 0.602 (Figure S3J). Proportional hazard regression showed the prognostic values of the four indices. No index showed significant prognostic values in univariable Cox regression either for OS or PFS, while a higher NLR was linked to shorter OS in multivariable Cox regression with hazard ratio 1.172 (95% CI, 1.0066–1.3639) (Figures S3K and S3L). Correspondingly, previous reports had shown the NLR as a negative prognostic factor in gastroesophageal junction and GAC.[17,34] Overall, the prognostic values of the four indices were limited.

Post-treatment tumor stromal PD-L1 level and pretreatment serum PD-L1 level both predict preoperative chemotherapy response

PD-L1 is a key immune-regulatory molecule. Upon interacting with its receptor, PD-1, PD-L1 suppresses the cytotoxic T cell immune response and thus participates in tumor immune escape. Choi et al., based on CLASSIC trial cohort, reported that the stromal PD-L1 level could predict benefit from adjuvant chemotherapy after D2 gastrectomy for stage II/III gastric cancer.[14] Utilizing a similar staining scoring system based on PD1/PDL1 immunohistochemistry (IHC) staining, we found the non-responders tended to have higher stromal PD-L1 staining scores in surgically resected tumor samples (Figures 4A and 4B). Stromal PD-1 staining showed a similar trend, though this was not statistically significant (Figures S4A and S4B). However, PD-L1 staining in tumor areas showed no correlation with treatment response (Figure 4A). These results showed that stromal PD-L1 levels in the tumors could predict preoperative chemotherapy response and indicated that PD-1/PD-L1 pathways may play a role in chemoresistance in gastric cancer.

However, the response predictive value of post-treatment stromal PD-L1 could be largely limited due to its lateness. An ideal predictor should be pretreatment. Stromal PD-L1 staining of pretreatment endoscopic biopsies was shown not able to

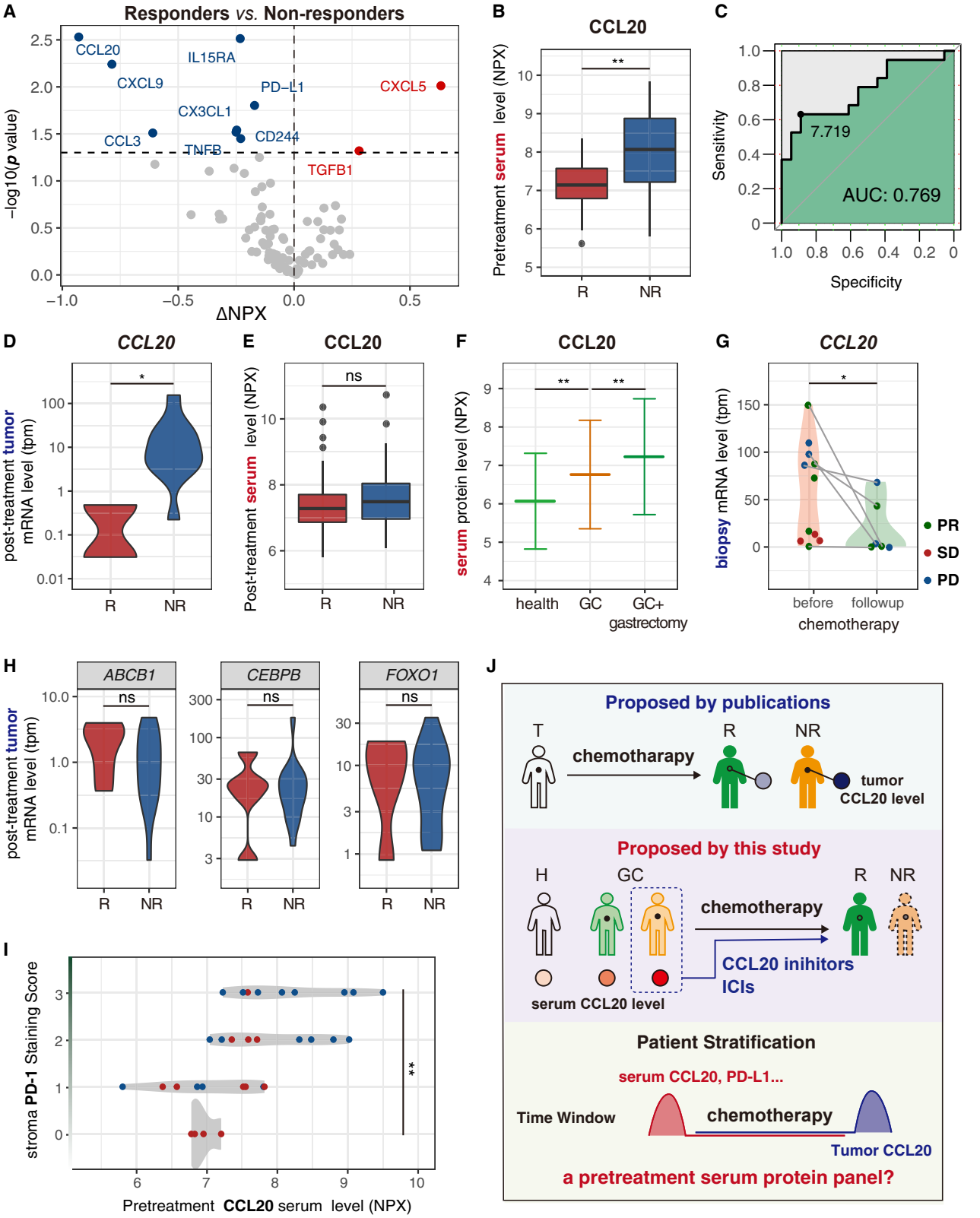

(legend on next page)

predict treatment response (Figures S4C and S4D). Thus, we further evaluated the clinical significance of pretreatment serum PD-L1 levels. Interestingly, pretreatment serum PD-L1 levels showed a difference in patients with different treatment responses (Figure 4C). Responders had lower serum PD-L1 levels before treatment, while treatment seemed to blunt this difference, as no significant difference was observed in post-treatment samples (Figure 4E). ROC curves were used to evaluate the response predictive value of pre- and post-treatment serum PD-L1 levels. AUC of pretreatment serum PD-L1 levels was 0.737 (95% CI, 0.569–0.904), while AUC of post-treatment serum PD-L1 levels was ~0.5 (Figures 4D and 4F), indicating that the pretreatment serum PD-L1 level was a promising response predictor of preoperative chemotherapies. Patients with high pretreatment serum PD-L1 levels (>5.084 normalized protein expression [NPX]) tended to show poorer response to preoperative chemotherapies (Figure S4E).

We also evaluated the on-treatment serum PD-L1 level of patients with different treatment responses. Serum PD-L1 seemed to increase during treatment in responders. The on-treatment serum PD-L1 level of responders was significantly higher (Figures S4F and S4G). One potential reason for this difference could be the destruction of tumor cells. More samples and further research were needed to confirm this finding and reveal potential mechanisms. Correlation between pathological PD-L1/PD-1 level and serum PD-L1 level was further measured. Among different pairs, pretreatment serum PD-L1 level and post-treatment stromal PD-1 level showed the strongest correlation (Figure S4H). The pretreatment serum PD-L1 level may link to the infiltration of PD-1$^+$ immune cells in tumors after chemotherapy.

Together, these results indicate that both the post-treatment tumor stromal PD-L1 level and pretreatment serum PD-L1 level could predict preoperative chemotherapy response while the pretreatment serum PD-L1 level should have greater clinical significance.

Pretreatment serum CCL20 level predicts response to preoperative chemotherapy

We further compared the pretreatment serum immune proteomics in patients with different treatment responses, inspired by the findings in PD-L1 (Figure 5A). Ten proteins showed a difference with $p < 0.05$. Among them, the pretreatment CCL20 level showed the most significant difference. Notably, we also compared the post-treatment serum immune proteomics in patients with different treatment responses, and the differences were much weaker compared with pretreatment samples (Figure S5A).

Recent publications have established CCL20 as an important mediator of chemoresistance in different cancers.[35–39] As summarized in Figure S5B, Chen et al. reported that chemotherapy induced CCL20 by a positive feedback loop between nuclear factor κB (NF-κB) and CCL20 and mediated chemoresistance by upregulating ATP-binding cassette subfamily B member 1 (ABCB1) expression in breast cancer. Wang et al. reported that chemotherapies upregulated CCL20 via FOXO1/CEBPB/NF-κB signaling in colorectal cancer cells and that secreted CCL20 recruited Tregs to promote chemoresistance. Liu et al. reported that cisplatin-stimulated classically activated macrophages (CAMs) promote ovarian cancer cell migration by increasing CCL20 production. Overall, existing publications indicate that CCL20 upregulation is induced by chemotherapy and that increased CCL20 production promotes chemoresistance.

However, our findings showed that the above model may not conserve in gastric cancer. We found that responders of preoperative chemotherapy had a significantly lower serum CCL20 level before the initiation of treatment (Figure 5B). The pretreatment serum CCL20 level predicted treatment response with an AUC of 0.769 (95% CI, 0.614–0.925) (Figure 5C) and indicated that patients with gastric cancer differed in serum CCL20 level before treatment. Consistent with existing publications, the CCL20 mRNA level was upregulated in tumors of non-responders (Figure 5D). However, post-treatment serum CCL20 levels showed no difference between responders and non-responders, indicating the decoupling of serum and tumor CCL20 levels (Figure 5E). Interestingly, referring to serum and tissue proteomics of resectable gastric cancer reported by Shen et al.,[40] we found that patients with gastric cancer tended to have higher serum CCL20 levels compared with healthy people (Figure 5F). Tumor samples also showed higher CCL20 protein levels compared with normal gastric tissues (Figure S5C). However, resection of tumors by gastrectomy did not recover serum CCL20 levels and instead further increased serum CCL20 levels (Figure 5F). These results indicate that serum CCL20 was not a systemic reflection of tumor CCL20 but an important component of systemic immunity toward gastric cancer and chemotherapy.

We also validated the signaling model of *CCL20* upregulation proposed by existing publications. Kim et al. collected the paired pretreatment and on-treatment gastric biopsy samples in treatment-naive patients undergoing first-line standard

Figure 5. Pretreatment serum CCL20 level predicts response to preoperative chemotherapy

(A) Comparison of pretreatment serum protein levels in responders (N = 18) and non-responders (N = 19).
(B) Responders (N = 18) had lower serum CCL20 level before treatment compared with non-responders (N = 19).
(C) ROC curve demonstrates the treatment response predictive accuracy of pretreatment serum CCL20 level.
(D) Responders (N = 6) had lower tumor *CCL20* mRNA level after chemotherapy compared with non-responders (N = 16). Data are represented by violin plot (*$p < 0.05$; t test).
(E) Post-treatment serum CCL20 level showed no difference between responders (N = 33) and non-responders (N = 50).
(F) Serum CCL20 level in healthy people and in patients with gastric cancer before and after gastrectomy.
(G) Biopsy tumor sample *CCL20* mRNA level decreased during chemotherapy in patients with gastric cancer.
(H) Post-treatment tumor *ABCB*, *CEBPB*, and *FOXO1* mRNA level showed no difference between responders (N = 33) and non-responders (N = 50).
(I) Higher pretreatment CCL20 level was linked to higher stromal PD-1 staining in post-treatment tumors.
(J) Patient stratification strategy proposed by publications in other cancer types and this study in gastric cancer.
See also Figure S5.

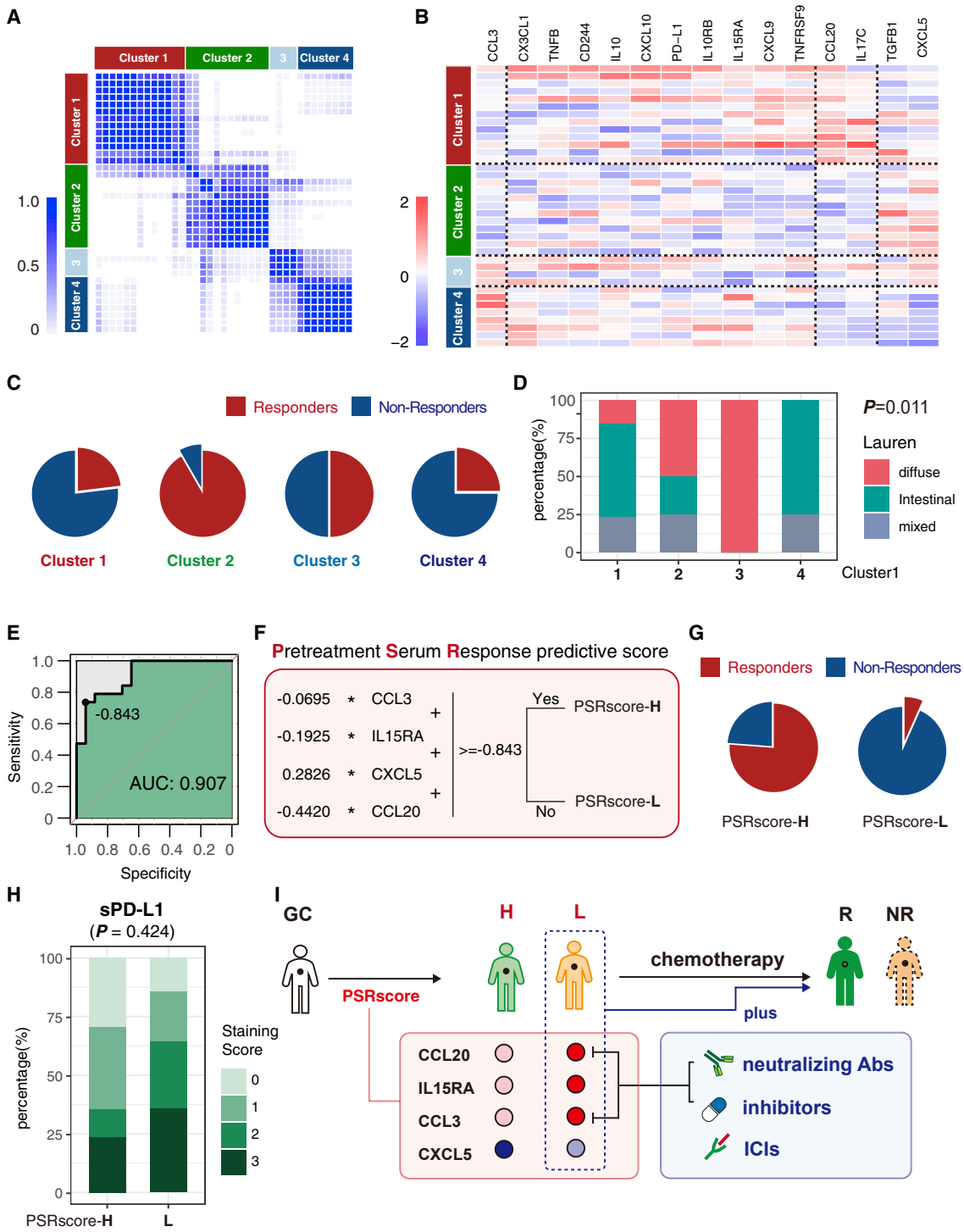

Figure 6. A pretreatment serum protein panel to predict the response to preoperative chemotherapy

(A) Unsupervised consensus clustering of pretreatment serum protein levels identified four clusters of patients.

(B) Pretreatment serum protein levels of four clusters.

(C) Treatment response in four clusters of patients.

(D) Lauren classification of tumors in four clusters of patients. p value was calculated by chi-squared test.

(E) ROC curve demonstrates treatment response predictive accuracy of pretreatment serum response predictive score (PSRscore).

(F) Formula of PSRscore.

(legend continued on next page)

chemotherapy without PD-1 blockade.[13] We analyzed their transcriptome data and found that chemotherapies did not increase *CCL20* mRNA level in tumor samples. Instead, *CCL20* mRNA level decreased after chemotherapy (Figure 5G). This finding challenged the assumption that *CCL20* upregulation was induced by chemotherapy in gastric cancer. Meanwhile, *ABCB1*, *CEBPB*, and *FOXO1* mRNA levels showed no difference either between the tumors with different responses (Figure 5H) or between biopsy samples before and after chemotherapy (Figure S5D). Rather, a higher pretreatment serum CCL20 level was linked to less infiltration of $CD4^+$ T cells in tumors (Figure S5E). $CD4^+$ T cells mediated immune response and were crucial in achieving a regulated and effective immune response to tumors. At the same time, higher pretreatment serum CCL20 levels correlated with more stromal infiltration of $PD\text{-}1^+$ or $PD\text{-}L1^+$ cells (Figures 5I and S5F), which should be key mediators of tumor immune escape. Together, these results demonstrated that serum CCL20 induced a systemic immunosuppressive environment for chemoresistance.

As summarized in Figure 5J, existing publications proposed that upregulation of *CCL20* in tumors was induced by chemotherapy and that increased CCL20 production promoted chemoresistance. However, we found that patients differed in serum CCL20 level before the initiation of chemotherapy. Patients with higher pretreatment serum CCL20 levels tended to have poorer treatment response. The potential mechanism is that serum CCL20 induced a systemic immunosuppressive environment. These findings suggest the combination of immunotherapy with chemotherapy in patients with high pretreatment serum CCL20 levels. Extensive effort had been devoted to developing inhibitors of the CCR6-CCL20 axis (CCR6 is the cellular receptor of CCL20).[37,41] Disruption of the CCR6-CCL20 axis by antibodies or antagonists has shown potential in cancer treatment. Pretreatment serum CCL20 levels may help pick patients who can potentially benefit from CCR6-CCL20 inhibitors. In addition, these findings showed that the pretreatment period was an irreplaceable time window for patient stratification by serum protein markers. We therefore decided to further establish a pretreatment serum protein panel for the prediction of preoperative chemotherapy response.

A pretreatment serum protein scoring system to predict the response to preoperative chemotherapy

Comparing pretreatment serum protein levels in patients with different treatment responses (Figure 5A), we included 15 proteins with $p < 0.1$ into consensus clustering. Based on the consensus cumulative distribution function (CDF) plot, delta area plot, and manual inspection of the consensus matrices, we found four pretreatment serum subtypes (Figures 6A, 6B, and S6A–S6H). Among them, cluster 2 was linked to a significantly better treatment response in patients (Figure 6C). This uncensored clustering was also associated with clinical characteristics of patients like the Lauren classification of tumors. Cluster 1 and 4 were linked to a higher proportion of intestinal-type adenocarcinoma (Figure 6D).

Taking clinical practicability into consideration, we further used the least absolute shrinkage and selection operator (LASSO) model to establish a pretreatment serum response predictive score (PSRscore) for the prediction of preoperative chemotherapy response (Figures S6I and S6J). Briefly, LASSO regression is a type of linear regression that uses shrinkage for variable selection or parameter elimination. With an appropriate λ value, the formula of PSRscore was limited to the serum levels of four proteins: CCL3, IL-15Rα), CXCL5, and CCL20 (Figures 6F and S6K). The ROC curve of PSRscore, with AUC 0.907 (95% CI, 0.814–1.000), determined the cutoff value to be −0.843 (Figure 6E). Patients were divided into PSRscore-high and -low groups (Figure 6F). A low PSRscore was linked to a significantly poorer treatment response (Figure 6G). In addition, patients with low PSRscores numerically have more stromal infiltration of $PD\text{-}1^+/PD\text{-}L1^+$ cells and higher tumor PD-L1 staining in post-treatment tumors (Figures 6H and S6L), which usually led to indications of anti-PD-1/PDL1 therapies.

Besides CCL20, pretreatment serum levels of CCL3, IL-15Rα, and CXCL5 were included in the PSRscore. Higher serum CCL3 and IL-15Rα levels and lower CXCL5 levels were linked to poorer treatment response (Figure S6K). Research has shown that CCL3 was involved in immune escape and chemoresistance in different cancers.[42] A high level of CCL3 was associated with increased intratumor infiltration of Tregs, tumor-associated macrophages (TAMs), and myeloid-derived suppressor cells (MDSCs).[43–45] CCL3-driven recruitment of TAMs has been recognized as a driver event in metastatic niches.[46] Neutralizing antibodies and inhibitors of CCL3 have been developed and have shown potential in anticancer treatment.[47–49] There is currently a limited understanding of the role of IL-15Rα and CXCL5 in chemoresistance. More work is needed to explore their functions in gastric cancer.

The PSRscore scoring system could help to stratify patents with GAC and screen out those who may not benefit from preoperative chemotherapies alone. For this group of patients, our work strongly implied that patients may benefit from a combination of immunotherapies such as ICIs or CCL3/20 neutralizing antibodies/inhibitors (Figure 6I). A prospective trial could be designed to validate this strategy, and a validation cohort would need to be established to validate the sensitivity and specificity of this scoring system.

The prognostic value of TME and serum immune proteomics

We further evaluated the prognostic value of the TME and serum immune proteomics. All basic clinical characteristics with predictive value in univariable Cox regression as well as age and gender were included in the multivariable Cox regression (Tables S2 and S3). Immune cells shown to be predictors of OS or PFS are listed in forest plots together with their hazard

(G) Treatment response in patients with high/low PSRscores.
(H) Post-treatment stromal PD-L1 level in patients with different PSRscores (high [H]: N = 18, low [L]: N = 14). p value was calculated by chi-squared test.
(I) The pretreatment patient stratification strategy based on PSRscore.
See also Figure S6.

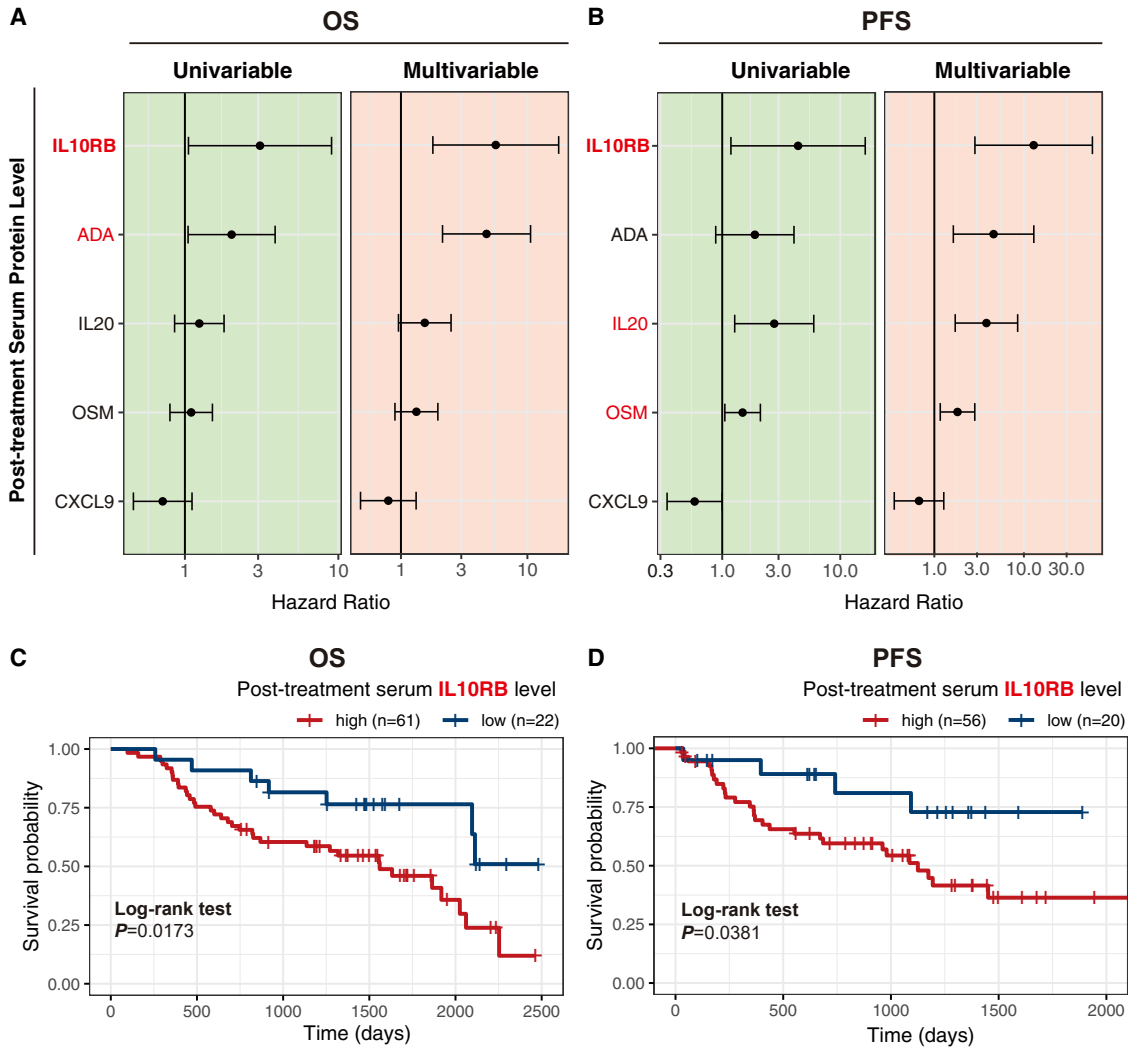

Figure 7. High post-treatment serum IL-10RB level predicted poor prognosis of patients having preoperative chemotherapy

(A) Hazard ratios (HRs) of post-treatment serum protein levels for overall survival (OS) calculated by univariable/multivariable cox regression.

(B) HRs of post-treatment serum protein levels for progression-free survival (PFS) calculated by univariable/multivariable Cox regression. The length of the horizontal line represented the 95% confidence interval of HR for each protein. The vertical solid line represented HR = 1.

(C) Kaplan-Meier curves of OS for patients with high (N = 61) and low (N = 22) post-treatment serum IL-10RB level. The p value of the log rank test is indicated.

(D) Kaplan-Meier curves of PFS for patients with high (N = 56) and low (N = 20) post-treatment serum IL-10RB level. The p value of the log rank test is indicated.

See also Figure S7 and Tables S1–S3.

ratios (Figures S7A and S7B). Kaplan-Meier curves of representative survival predictors were drawn (Figures S7C–S7F). No immune cell types were independent prognostic factors of OS, while the infiltration of $CD68^+$ macrophages predicted shorter PFS confirmed by log rank test, univariable Cox regression, and multivariable Cox regression (Figure S7C). Infiltration of $CD68^+$ macrophages was also shown to be a negative prognostic factor of OS by log rank test, though not independent (Figure S7D).

Post- and pretreatment serum proteins shown to be predictors of OS or PFS were also listed in forest plots together with their hazard ratios (Figures 7A, 7B, S7G, and S7H). Kaplan-Meier curves of representative survival predictors were drawn (Figures 7C, 7D, S7I, and S7J). Among them, high post-treatment serum IL-10RB level was linked to both significantly shorter OS and PFS, confirmed by log rank test, univariable cox regression, and multivariable cox regression (Figures 7C and 7D). This indicated that the post-treatment serum IL-10RB level was a strong negative survival predictor for patients having preoperative chemotherapy. Notably, the serum IL-10RB level showed a significant increase after preoperative chemotherapies, indicating its potential participation in preoperative chemotherapy responses (Figure S1D). Reports about the role of IL-10 signaling in gastric cancer have been limited. More work is needed to

understand the role of IL-10RB in gastric cancer preoperative treatment.

DISCUSSION

In the last decade, efforts have been devoted to revealing the role of immunity in cancer. Immunotherapy brought breakthroughs in gastric cancer treatment, and ICIs became first-line treatment of advanced gastric or esophageal adenocarcinoma (GEAC).[50] However, no treatment has successfully challenged the backbone status of chemotherapies in the perioperative treatment of gastric cancers. Immunity is thought to play a key role in patients benefiting from perioperative chemotherapy.[11–13,24] However, existing studies have focused heavily on local immune responses in the TME. An improved understanding of immunity in gastric cancer must assess, in particular, systemic immunity. We used serum immune proteomics and classic systemic immune-inflammation indices to profile systemic immunity and studied its associations with the TME as well as treatment response. We found that preoperative treatment induced sophisticated systemic immune responses indicated by dynamic immune proteomics. Meanwhile, patients with better treatment response showed a more dynamic change of serum immune proteomics after treatment. TME was also shown to be associated with the response to preoperative chemotherapy. However, it will be more practical to a predict potential response before treatment is administrated. Excitingly, we found that pretreatment serum levels of PD-L1 and CCL20 were predictors of preoperative chemotherapy responses, consistent with their known roles in immunosuppression. A pretreatment serum protein panel was further established for response prediction, which was able to precisely screen out patients who may not respond to preoperative chemotherapies alone. As to this part of patients, we believed they would benefit from the combination of immunotherapy and chemotherapy. The post-treatment serum level of IL-10RB was also established as a strong predictor of prognosis for patients with gastric cancer.

The role of intratumoral PD-L1 in immunosuppression and chemoresistance has been well established. However, the studies in soluble PD-L1 were limited. Our work found that serum PD-L1 levels had differed in patients before the initiation of chemotherapy. Patients responding to chemotherapies tended to have lower serum PD-L1 levels. More work is needed to explore whether soluble PD-L1 plays a role in chemoresistance. Similar findings were found in CCL20, a chemokine known to participate in chemoresistance in various cancer types. Our work showed that the existing model of CCL20-induced chemoresistance proposed in other cancer types may not conserve in gastric cancer. The view that the alternation of CCL20 was a consequence of chemotherapies deprived the initiative of clinicians to stratify and intervene patients ahead of treatments. Our findings, instead, showed that patients with different treatment responses have differed in serum immune proteomics before the initiation of chemotherapy, which brought forward the time window of patient stratification and intervention. Inspired by PD-L1 and CCL20, we developed a pretreatment serum protein panel for the prediction of preoperative chemotherapy response called the PSRscore. By calculating the pretreatment serum protein level of four immune proteins, patients could be stratified into two groups. The PSRscore-low group tended to have poorer treatment response and may benefit from the combination of immunotherapies. This scoring system has great potentials of clinical translation for patient stratification. Notably, the establishment of the PSRscore was based on an Asian cohort receiving platinum-based chemotherapies. How these immune markers will perform in non-Asian patients receiving Taxol-based regimens needs to be further validated.

We believed that serum protein biomarkers have special clinical significance in the pretreatment stratification of patients with gastric cancer. Almost all the existing molecular classifications of gastric cancer depended on surgically or endoscopically resected tumor tissues. With TCGA classification as the most famous example, microsatellite instability (MSI)-type patients were shown to benefit more from immunotherapies, while genomically stable (GS)-type patients responded poorly to chemotherapies.[51,52] However, these molecular classifications are rarely used in clinical practice. One important reason would be that most molecular classifications depend on sophisticated molecular technologies such as qPCR, *in situ* hybridization, or even omics technologies, which are not accessible in most clinics. Besides, obtaining tumor samples before operations is dependent on gastroscopic biopsies in gastric cancer. Significant intratumoral heterogeneity of gastric cancer and limited biopsy depth largely impair the representation of biopsy samples.[53–56] Determining molecular classifications of gastric cancer has thus been quite difficult before gastrectomy. Comparably, serum proteomics incorporate both the systemic and tumor local features and are thus sensitive and informative. Serum samples can be easily obtained in clinics with limited harm to patients. Serum protein biomarkers like prostate-specific antigen (PSA) or α-fetoprotein (AFP) have been used in the diagnosis and follow up of cancer for decades. Devices and trainees for the measurement of serum proteins are widely available in various hospitals. These factors endow the studies in serum proteomics of gastric cancer with great clinical significance. A serum protein classification of gastric cancer should be established in the future to guide perioperative treatment of gastric cancer.

Limitations of the study

There are some limitations of the study that should be noted. First, the number of on-treatment serum samples was relatively small, which limited the statistical power to draw some conclusions. Second, mIF only measured key immune cells in the TME. Single-cell sequencing could be used for better profiling of the TME. Third, some conclusions and proposals of this study should be further validated in a prospective cohort of patients receiving preoperative chemotherapy or even a randomized controlled trial. These limitations should be taken into consideration when interpreting the data.

In summary, we profiled both systemic immunity and the TME in patients with gastric cancer and showed their association with preoperative chemotherapy response. Serum biomarkers were identified for the prediction of treatment response and prognosis. This work emphasized the fundamental, but largely underestimated, role of systemic immunity in the preoperative chemotherapy of gastric cancer, supporting a patient stratification

strategy based on pretreatment serum immune proteomics and highlighting the importance of profiling immunity as a whole in future studies.

STAR★METHODS

Detailed methods are provided in the online version of this paper and include the following:

- KEY RESOURCES TABLE
- RESOURCE AVAILABILITY
  - Lead contact
  - Materials availability
  - Data and code availability
- EXPERIMENTAL MODEL AND SUBJECT DETAILS
  - Study cohort
- METHOD DETAILS
  - Serum immune proteomics
  - PD-1/PD-L1 immunohistochemistry staining
  - Multiplex immunofluorescence
  - RNA sequencing
  - Classic systemic immune-inflammation indices
  - Consensus clustering and LASSO regression
- QUANTIFICATION AND STATISTICAL ANALYSIS

SUPPLEMENTAL INFORMATION

Supplemental information can be found online at https://doi.org/10.1016/j.xcrm.2023.100931.

ACKNOWLEDGMENTS

We would like to acknowledge Professor Fa-xing Yu (Fudan University, China), Professor Zhifang Ren (Fudan University, China), and Dr. Zhaoming Wang (Zhongshan Hospital, Fudan University, China) for reviewing the paper and providing advice. We would like to thank Dr. Karen Tumaneng for proofreading and comments. This work was supported in part by the National Natural Science Foundation of China (to Y.S., 81872425; to X.W., 81972228), Shanghai Pu Jiang Talents plan (to X.W., 2019PJD005), and Shanghai "Science and Technology Innovation Action Plan" Project (to Y.C., 21SQBS00200).

AUTHOR CONTRIBUTIONS

Z.T., Y.G., Y.C., Y.S., and X.W. designed the study; Z.S., L.M., Z.Z., and P.Z. enrolled patients and collected samples; R.L. performed pathologic evaluation; Y.W. and Y.C. performed drug administration; Y.S. supervised surgeries; Z.T. and Y.G. collected data and performed data analysis; Z.T., Y.G., and X.W. drafted and revised the manuscript; Y.C., Y.S., and X.W. led the project.

DECLARATION OF INTERESTS

The authors declare no competing interests.

Received: June 20, 2022
Revised: August 23, 2022
Accepted: January 11, 2023
Published: January 31, 2023

REFERENCES

1. Bray, F., Ferlay, J., Soerjomataram, I., Siegel, R.L., Torre, L.A., and Jemal, A. (2018). Global cancer statistics 2018: GLOBOCAN estimates of incidence and mortality worldwide for 36 cancers in 185 countries. CA. Cancer J. Clin. *68*, 394–424. https://doi.org/10.3322/caac.21492.
2. Ajani, J.A., Lee, J., Sano, T., Janjigian, Y.Y., Fan, D., and Song, S. (2017). Gastric adenocarcinoma. Nat. Rev. Dis. Primers *3*, 17036. https://doi.org/10.1038/nrdp.2017.36.
3. Katai, H., Ishikawa, T., Akazawa, K., Isobe, Y., Miyashiro, I., Oda, I., Tsujitani, S., Ono, H., Tanabe, S., Fukagawa, T., et al. (2018). Five-year survival analysis of surgically resected gastric cancer cases in Japan: a retrospective analysis of more than 100,000 patients from the nationwide registry of the Japanese Gastric Cancer Association (2001-2007). Gastric Cancer *21*, 144–154. https://doi.org/10.1007/s10120-017-0716-7.
4. Sano, T., Sasako, M., Mizusawa, J., Yamamoto, S., Katai, H., Yoshikawa, T., Nashimoto, A., Ito, S., Kaji, M., Imamura, H., et al. (2017). Randomized controlled trial to evaluate splenectomy in total gastrectomy for proximal gastric carcinoma. Ann. Surg. *265*, 277–283. https://doi.org/10.1097/SLA.0000000000001814.
5. Sasako, M., Sano, T., Yamamoto, S., Sairenji, M., Arai, K., Kinoshita, T., Nashimoto, A., and Hiratsuka, M.; Japan Clinical Oncology Group JCOG9502 (2006). Left thoracoabdominal approach versus abdominal-transhiatal approach for gastric cancer of the cardia or subcardia: a randomised controlled trial. Lancet Oncol. *7*, 644–651. https://doi.org/10.1016/S1470-2045(06)70766-5.
6. Tsujinaka, T., Sasako, M., Yamamoto, S., Sano, T., Kurokawa, Y., Nashimoto, A., Kurita, A., Katai, H., Shimizu, T., Furukawa, H., et al. (2007). Influence of overweight on surgical complications for gastric cancer: results from a randomized control trial comparing D2 and extended para-aortic D3 lymphadenectomy (JCOG9501). Ann. Surg Oncol. *14*, 355–361. https://doi.org/10.1245/s10434-006-9209-3.
7. Cunningham, D., Allum, W.H., Stenning, S.P., Thompson, J.N., Van de Velde, C.J.H., Nicolson, M., Scarffe, J.H., Lofts, F.J., Falk, S.J., Iveson, T.J., et al. (2006). Perioperative chemotherapy versus surgery alone for resectable gastroesophageal cancer. N. Engl. J. Med. *355*, 11–20. https://doi.org/10.1056/NEJMoa055531.
8. Al-Batran, S.E., Hofheinz, R.D., Pauligk, C., Kopp, H.G., Haag, G.M., Luley, K.B., Meiler, J., Homann, N., Lorenzen, S., Schmalenberg, H., et al. (2016). Histopathological regression after neoadjuvant docetaxel, oxaliplatin, fluorouracil, and leucovorin versus epirubicin, cisplatin, and fluorouracil or capecitabine in patients with resectable gastric or gastro-oesophageal junction adenocarcinoma (FLOT4-AIO): results from the phase 2 part of a multicentre, open-label, randomised phase 2/3 trial. Lancet Oncol. *17*, 1697–1708. https://doi.org/10.1016/S1470-2045(16)30531-9.
9. Al-Batran, S.E., Homann, N., Pauligk, C., Goetze, T.O., Meiler, J., Kasper, S., Kopp, H.G., Mayer, F., Haag, G.M., Luley, K., et al. (2019). Perioperative chemotherapy with fluorouracil plus leucovorin, oxaliplatin, and docetaxel versus fluorouracil or capecitabine plus cisplatin and epirubicin for locally advanced, resectable gastric or gastro-oesophageal junction adenocarcinoma (FLOT4): a randomised, phase 2/3 trial. Lancet *393*, 1948–1957. https://doi.org/10.1016/S0140-6736(18)32557-1.
10. Smyth, E.C., Nilsson, M., Grabsch, H.I., van Grieken, N.C., and Lordick, F. (2020). Gastric cancer. Lancet *396*, 635–648. https://doi.org/10.1016/S0140-6736(20)31288-5.
11. Li, Z., Gao, X., Peng, X., May Chen, M.J., Li, Z., Wei, B., Wen, X., Wei, B., Dong, Y., Bu, Z., et al. (2020). Multi-omics characterization of molecular features of gastric cancer correlated with response to neoadjuvant chemotherapy. Sci. Adv. *6*, eaay4211. https://doi.org/10.1126/sciadv.aay4211.
12. Choi, Y.Y., Kim, H., Shin, S.J., Kim, H.Y., Lee, J., Yang, H.K., Kim, W.H., Kim, Y.W., Kook, M.C., Park, Y.K., et al. (2019). Microsatellite instability and programmed cell death-ligand 1 expression in stage II/III gastric cancer: post Hoc analysis of the CLASSIC randomized controlled study. Ann. Surg. *270*, 309–316. https://doi.org/10.1097/SLA.0000000000002803.
13. Kim, R., An, M., Lee, H., Mehta, A., Heo, Y.J., Kim, K.M., Lee, S.Y., Moon, J., Kim, S.T., Min, B.H., et al. (2021). Early tumor-immune microenvironmental remodeling and response to frontline fluoropyrimidine and

platinum chemotherapy in advanced gastric cancer. Cancer Discov. *12*, 984–1001. https://doi.org/10.1158/2159-8290.CD-21-0888.

14. Hiam-Galvez, K.J., Allen, B.M., and Spitzer, M.H. (2021). Systemic immunity in cancer. Nat. Rev. Cancer *21*, 345–359. https://doi.org/10.1038/s41568-021-00347-z.
15. Rumble, J.M., Huber, A.K., Krishnamoorthy, G., Srinivasan, A., Giles, D.A., Zhang, X., Wang, L., and Segal, B.M. (2015). Neutrophil-related factors as biomarkers in EAE and MS. J. Exp. Med. *212*, 23–35. https://doi.org/10.1084/jem.20141015.
16. Schiefer, S., Wirsik, N.M., Kalkum, E., Seide, S.E., Nienhüser, H., Müller, B., Billeter, A., Büchler, M.W., Schmidt, T., and Probst, P. (2022). Systematic Review of prognostic role of blood cell ratios in patients with gastric cancer undergoing surgery. Diagnostics *12*, 593. https://doi.org/10.3390/diagnostics12030593.
17. Wang, S.C., Chou, J.F., Strong, V.E., Brennan, M.F., Capanu, M., and Coit, D.G. (2016). Pretreatment neutrophil to lymphocyte ratio independently predicts disease-specific survival in resectable gastroesophageal junction and gastric adenocarcinoma. Ann. Surg. *263*, 292–297. https://doi.org/10.1097/SLA.0000000000001189.
18. Chen, B., Scurrah, C.R., McKinley, E.T., Simmons, A.J., Ramirez-Solano, M.A., Zhu, X., Markham, N.O., Heiser, C.N., Vega, P.N., Rolong, A., et al. (2021). Differential pre-malignant programs and microenvironment chart distinct paths to malignancy in human colorectal polyps. Cell *184*, 6262–6280.e26. https://doi.org/10.1016/j.cell.2021.11.031.
19. Lee, J.W.J., Plichta, D., Hogstrom, L., Borren, N.Z., Lau, H., Gregory, S.M., Tan, W., Khalili, H., Clish, C., Vlamakis, H., et al. (2021). Multi-omics reveal microbial determinants impacting responses to biologic therapies in inflammatory bowel disease. Cell Host Microbe *29*, 1294–1304.e4. https://doi.org/10.1016/j.chom.2021.06.019.
20. Pelka, K., Hofree, M., Chen, J.H., Sarkizova, S., Pirl, J.D., Jorgji, V., Bejnood, A., Dionne, D., Ge, W.H., Xu, K.H., et al. (2021). Spatially organized multicellular immune hubs in human colorectal cancer. Cell *184*, 4734–4752.e20. https://doi.org/10.1016/j.cell.2021.08.003.
21. Ramaswamy, A., Brodsky, N.N., Sumida, T.S., Comi, M., Asashima, H., Hoehn, K.B., Li, N., Liu, Y., Shah, A., Ravindra, N.G., et al. (2021). Immune dysregulation and autoreactivity correlate with disease severity in SARS-CoV-2-associated multisystem inflammatory syndrome in children. Immunity *54*, 1083–1095.e7. https://doi.org/10.1016/j.immuni.2021.04.003.
22. Sun, B.B., Maranville, J.C., Peters, J.E., Stacey, D., Staley, J.R., Blackshaw, J., Burgess, S., Jiang, T., Paige, E., Surendran, P., et al. (2018). Genomic atlas of the human plasma proteome. Nature *558*, 73–79. https://doi.org/10.1038/s41586-018-0175-2.
23. Zhou, Z., Xia, G., Xiang, Z., Liu, M., Wei, Z., Yan, J., Chen, W., Zhu, J., Awasthi, N., Sun, X., et al. (2019). A C-X-C chemokine receptor type 2-dominated cross-talk between tumor cells and macrophages drives gastric cancer metastasis. Clin. Cancer Res. *25*, 3317–3328. https://doi.org/10.1158/1078-0432.CCR-18-3567.
24. Xing, X., Shi, J., Jia, Y., Dou, Y., Li, Z., Dong, B., Guo, T., Cheng, X., Li, X., Du, H., et al. (2022). Effect of neoadjuvant chemotherapy on the immune microenvironment in gastric cancer as determined by multiplex immunofluorescence and T cell receptor repertoire analysis. J. Immunother. Cancer *10*, e003984. https://doi.org/10.1136/jitc-2021-003984.
25. Chen, J., Wang, H., Jia, L., He, J., Li, Y., Liu, H., Wu, R., Qiu, Y., Zhan, Y., Yuan, Z., et al. (2021). Bufalin targets the SRC-3/MIF pathway in chemoresistant cells to regulate M2 macrophage polarization in colorectal cancer. Cancer Lett. *513*, 63–74. https://doi.org/10.1016/j.canlet.2021.05.008.
26. Chung, A.W., Anand, K., Anselme, A.C., Chan, A.A., Gupta, N., Venta, L.A., Schwartz, M.R., Qian, W., Xu, Y., Zhang, L., et al. (2021). A phase 1/2 clinical trial of the nitric oxide synthase inhibitor L-NMMA and taxane for treating chemoresistant triple-negative breast cancer. Sci. Transl. Med. *13*, eabj5070. https://doi.org/10.1126/scitranslmed.abj5070.
27. Genin, M., Clement, F., Fattaccioli, A., Raes, M., and Michiels, C. (2015). M1 and M2 macrophages derived from THP-1 cells differentially modulate the response of cancer cells to etoposide. BMC Cancer *15*, 577. https://doi.org/10.1186/s12885-015-1546-9.
28. Song, M., Liu, T., Shi, C., Zhang, X., and Chen, X. (2016). Bioconjugated manganese dioxide nanoparticles enhance chemotherapy response by priming tumor-associated macrophages toward M1-like phenotype and attenuating tumor hypoxia. ACS Nano *10*, 633–647. https://doi.org/10.1021/acsnano.5b06779.
29. Wilson, A.J., Saskowski, J., Barham, W., Khabele, D., and Yull, F. (2015). Microenvironmental effects limit efficacy of thymoquinone treatment in a mouse model of ovarian cancer. Mol. Cancer *14*, 192. https://doi.org/10.1186/s12943-015-0463-5.
30. Travis, M.A., and Sheppard, D. (2014). TGF-beta activation and function in immunity. Annu. Rev. Immunol. *32*, 51–82. https://doi.org/10.1146/annurev-immunol-032713-120257.
31. Wang, R., and Huang, K. (2020). CCL11 increases the proportion of CD4+CD25+Foxp3+ Treg cells and the production of IL-2 and TGF-β by CD4+ T cells via the STAT5 signaling pathway. Mol. Med. Rep. *21*, 2522–2532. https://doi.org/10.3892/mmr.2020.11049.
32. Olaloye, O.O., Liu, P., Toothaker, J.M., McCourt, B.T., McCourt, C.C., Xiao, J., Prochaska, E., Shaffer, S., Werner, L., et al.; UPMC NICU Faculty (2021). CD16+CD163+ monocytes traffic to sites of inflammation during necrotizing enterocolitis in premature infants. J. Exp. Med. *218*, e20200344. https://doi.org/10.1084/jem.20200344.
33. Paudel, S., Baral, P., Ghimire, L., Bergeron, S., Jin, L., DeCorte, J.A., Le, J.T., Cai, S., and Jeyaseelan, S. (2019). CXCL1 regulates neutrophil homeostasis in pneumonia-derived sepsis caused by Streptococcus pneumoniae serotype 3. Blood *133*, 1335–1345. https://doi.org/10.1182/blood-2018-10-878082.
34. Grenader, T., Waddell, T., Peckitt, C., Oates, J., Starling, N., Cunningham, D., and Bridgewater, J. (2016). Prognostic value of neutrophil-to-lymphocyte ratio in advanced oesophago-gastric cancer: exploratory analysis of the REAL-2 trial. Ann. Oncol. *27*, 687–692. https://doi.org/10.1093/annonc/mdw012.
35. Chen, W., Qin, Y., Wang, D., Zhou, L., Liu, Y., Chen, S., Yin, L., Xiao, Y., Yao, X.H., Yang, X., et al. (2018). CCL20 triggered by chemotherapy hinders the therapeutic efficacy of breast cancer. PLoS Biol. *16*, e2005869. https://doi.org/10.1371/journal.pbio.2005869.
36. Liu, W., Wang, W., Wang, X., Xu, C., Zhang, N., and Di, W. (2020). Cisplatin-stimulated macrophages promote ovarian cancer migration via the CCL20-CCR6 axis. Cancer Lett. *472*, 59–69. https://doi.org/10.1016/j.canlet.2019.12.024.
37. Ranasinghe, R., and Eri, R. (2018). Modulation of the CCR6-CCL20 Axis: a potential therapeutic target in inflammation and cancer. Medicina (Kaunas) *54*, 88. https://doi.org/10.3390/medicina54050088.
38. Su, S., Sun, X., Zhang, Q., Zhang, Z., and Chen, J. (2019). CCL20 promotes ovarian cancer chemotherapy resistance by regulating ABCB1 expression. Cell Struct. Funct. *44*, 21–28. https://doi.org/10.1247/csf.18029.
39. Wang, D., Yang, L., Yu, W., Wu, Q., Lian, J., Li, F., Liu, S., Li, A., He, Z., Liu, J., et al. (2019). Colorectal cancer cell-derived CCL20 recruits regulatory T cells to promote chemoresistance via FOXO1/CEBPB/NF-κB signaling. J. Immunother. Cancer *7*, 215. https://doi.org/10.1186/s40425-019-0701-2.
40. Shen, Q., Polom, K., Williams, C., de Oliveira, F.M.S., Guergova-Kuras, M., Lisacek, F., Karlsson, N.G., Roviello, F., and Kamali-Moghaddam, M. (2019). A targeted proteomics approach reveals a serum protein signature as diagnostic biomarker for resectable gastric cancer. EBioMedicine *44*, 322–333. https://doi.org/10.1016/j.ebiom.2019.05.044.
41. Meitei, H.T., Jadhav, N., and Lal, G. (2021). CCR6-CCL20 axis as a therapeutic target for autoimmune diseases. Autoimmun. Rev. *20*, 102846. https://doi.org/10.1016/j.autrev.2021.102846.

42. Ntanasis-Stathopoulos, I., Fotiou, D., and Terpos, E. (2020). CCL3 signaling in the tumor microenvironment. Adv. Exp. Med. Biol. *1231*, 13–21. https://doi.org/10.1007/978-3-030-36667-4_2.

43. Chen, D., and Bromberg, J.S. (2006). T regulatory cells and migration. Am. J. Transplant. *6*, 1518–1523. https://doi.org/10.1111/j.1600-6143.2006.01372.x.

44. Murdoch, C., Muthana, M., Coffelt, S.B., and Lewis, C.E. (2008). The role of myeloid cells in the promotion of tumour angiogenesis. Nat. Rev. Cancer *8*, 618–631. https://doi.org/10.1038/nrc2444.

45. Chanmee, T., Ontong, P., Konno, K., and Itano, N. (2014). Tumor-associated macrophages as major players in the tumor microenvironment. Cancers *6*, 1670–1690. https://doi.org/10.3390/cancers6031670.

46. Argyle, D., and Kitamura, T. (2018). Targeting macrophage-recruiting chemokines as a novel therapeutic strategy to prevent the progression of solid tumors. Front. Immunol. *9*, 2629. https://doi.org/10.3389/fimmu.2018.02629.

47. Ackun-Farmmer, M.A., Soto, C.A., Lesch, M.L., Byun, D., Yang, L., Calvi, L.M., Benoit, D.S.W., and Frisch, B.J. (2021). Reduction of leukemic burden via bone-targeted nanoparticle delivery of an inhibitor of C-chemokine (C-C motif) ligand 3 (CCL3) signaling. FASEB J *35*, e21402. https://doi.org/10.1096/fj.202000938RR.

48. Wang, J., Ortiz, C., Fontenot, L., Mukhopadhyay, R., Xie, Y., Chen, X., Feng, H., Pothoulakis, C., and Koon, H.W. (2020). Therapeutic mechanism of macrophage inflammatory protein 1 alpha neutralizing antibody (CCL3) in Clostridium difficile infection in mice. J. Infect. Dis. *221*, 1623–1635. https://doi.org/10.1093/infdis/jiz640.

49. Sayeed, H.M., Lee, E.S., Byun, H.O., and Sohn, S. (2019). The role of CCR1 and therapeutic effects of anti-CCL3 antibody in herpes simplex virus-induced Behcet's disease mouse model. Immunology *158*, 206–218. https://doi.org/10.1111/imm.13102.

50. Joshi, S.S., and Badgwell, B.D. (2021). Current treatment and recent progress in gastric cancer. CA. Cancer J. Clin. *71*, 264–279. https://doi.org/10.3322/caac.21657.

51. Cancer Genome Atlas Research Network (2014). Comprehensive molecular characterization of gastric adenocarcinoma. Nature *513*, 202–209. https://doi.org/10.1038/nature13480.

52. Chia, N.Y., and Tan, P. (2016). Molecular classification of gastric cancer. Ann. Oncol. *27*, 763–769. https://doi.org/10.1093/annonc/mdw040.

53. Sathe, A., Grimes, S.M., Lau, B.T., Chen, J., Suarez, C., Huang, R.J., Poultsides, G., and Ji, H.P. (2020). Single-cell genomic characterization reveals the cellular reprogramming of the gastric tumor microenvironment. Clin. Cancer Res. *26*, 2640–2653. https://doi.org/10.1158/1078-0432.CCR-19-3231.

54. Sundar, R., Liu, D.H., Hutchins, G.G., Slaney, H.L., Silva, A.N., Oosting, J., Hayden, J.D., Hewitt, L.C., Ng, C.C., Mangalvedhekar, A., et al. (2021). Spatial profiling of gastric cancer patient-matched primary and locoregional metastases reveals principles of tumour dissemination. Gut *70*, 1823–1832. https://doi.org/10.1136/gutjnl-2020-320805.

55. von Loga, K., Woolston, A., Punta, M., Barber, L.J., Griffiths, B., Semiannikova, M., Spain, G., Challoner, B., Fenwick, K., Simon, R., et al. (2020). Extreme intratumour heterogeneity and driver evolution in mismatch repair deficient gastro-oesophageal cancer. Nat. Commun. *11*, 139. https://doi.org/10.1038/s41467-019-13915-7.

56. Wang, R., Dang, M., Harada, K., Han, G., Wang, F., Pool Pizzi, M., Zhao, M., Tatlonghari, G., Zhang, S., Hao, D., et al. (2021). Single-cell dissection of intratumoral heterogeneity and lineage diversity in metastatic gastric adenocarcinoma. Nat. Med. *27*, 141–151. https://doi.org/10.1038/s41591-020-1125-8.

57. Becker, K., Mueller, J.D., Schulmacher, C., Ott, K., Fink, U., Busch, R., Böttcher, K., Siewert, J.R., and Höfler, H. (2003). Histomorphology and grading of regression in gastric carcinoma treated with neoadjuvant chemotherapy. Cancer *98*, 1521–1530. https://doi.org/10.1002/cncr.11660.

58. Assarsson, E., Lundberg, M., Holmquist, G., Björkesten, J., Thorsen, S.B., Ekman, D., Eriksson, A., Rennel Dickens, E., Ohlsson, S., Edfeldt, G., et al. (2014). Homogenous 96-plex PEA immunoassay exhibiting high sensitivity, specificity, and excellent scalability. PLoS One *9*, e95192. https://doi.org/10.1371/journal.pone.0095192.

59. Ebai, T., Kamali-Moghaddam, M., and Landegren, U. (2015). Parallel protein detection by solid-phase proximity ligation assay with real-time PCR or sequencing. Curr. Protoc. Mol. Biol. *109*, 20.10.1–20.10.25. https://doi.org/10.1002/0471142727.mb2010s109.

60. Love, M.I., Huber, W., and Anders, S. (2014). Moderated estimation of fold change and dispersion for RNA-seq data with DESeq2. Genome Biol. *15*, 550. https://doi.org/10.1186/s13059-014-0550-8.

61. Yu, G., Wang, L.G., Han, Y., and He, Q.Y. (2012). clusterProfiler: an R package for comparing biological themes among gene clusters. OMICS *16*, 284–287. https://doi.org/10.1089/omi.2011.0118.

62. Wilkerson, M.D., and Hayes, D.N. (2010). ConsensusClusterPlus: a class discovery tool with confidence assessments and item tracking. Bioinformatics *26*, 1572–1573. https://doi.org/10.1093/bioinformatics/btq170.

63. Friedman, J., Hastie, T., and Tibshirani, R. (2010). Regularization paths for generalized linear models via coordinate descent. J. Stat. Softw. *33*, 1–22.

STAR★METHODS

KEY RESOURCES TABLE

REAGENT or RESOURCE	SOURCE	IDENTIFIER
Antibodies		
Rabbit monoclonal anti-PD1(EPR4877(2))	Abcam	Cat#ab137132; RRID: AB_2894867
Rabbit monoclonal anti-PD-L1(SP142)	Abcam	Cat#ab228462; RRID: AB_2827816
Rabbit polyclonal anti-FOXP3	Servicebio	Cat#GB112325; RRID: AB_2922969
Mouse monoclonal anti-CD163	Servicebio	Cat#GB14027; RRID: AB_2892095
Rabbit polyclonal anti-CD68	Servicebio	Cat# GB113150; RRID: AB_2924885
Rabbit polyclonal anti-CD4	Servicebio	Cat#GB11064; RRID: AB_2904187
Mouse monoclonal anti-CD8	Servicebio	Cat#GB12068; RRID: AB_2905512
Critical commercial assays		
RNeasy Plus mini kit	Qiagen	Cat#74134
TruSeq RNA Sample Preparation Kit	Illumina	Cat#FC-122-1001
Deposited data		
Human serum proteomics data	This study	NGDC: OMIX001800
Gastric cancer transcriptome data	This study	NGDC: OMIX001799
Software and algorithms		
R	Bell Laboratories	https://www.r-project.org
GraphPad Prism 8	GraphPad	https://www.graphpad.com/scientific-software/prism/
HALO	Indica Labs	https://www.indicalab.com/halo
PANNORAMIC MIDI II automatic digital slide scanner system	3dhistech	www.3dhistech.com

RESOURCE AVAILABILITY

Lead contact

Further information and requests for resources and reagents should be directed to and will be fulfilled by the lead contact, Xuefei Wang (wang.xuefei@zs-hospital.sh.cn).

Materials availability

This study did not generate new, unique reagents.

Data and code availability

All raw data generated by this study have been deposited in the Chinese national genomics data center (https://ngdc.cncb.ac.cn), under accession number NGDC: OMIX001799 and OMIX001800, which are publicly accessible. Additional data related to this paper may be requested from the authors. Public datasets used in this study were downloaded from resources as described in primary manuscripts.[13,40]

This paper does not report original code.

Any additional information required to reanalyze the data reported in this paper is available from the lead contact upon request.

EXPERIMENTAL MODEL AND SUBJECT DETAILS

Study cohort

This study included ninety gastric adenocarcinoma patients who underwent gastrectomy after preoperative chemotherapy in Zhongshan Hospital of Fudan University (Shanghai, China) from 2016 to 2019. Key eligibility criteria included (1) pathological diagnosis of gastric adenocarcinoma with available serum samples, frozen tissues, formalin fixation and paraffin embedding (FFPE) tissues, and follow-up information; (2) received at least two cycles of standard preoperative chemotherapies before gastrectomy without ICIs. (3) eligible serum samples at $\geq$1 timepoint. (4) No other significant systemic diseases including autoimmune disorders. (5) not involved

in previous procedures. Patients were retrospectively involved and 90 patients met the eligibility criteria. The basic clinical characteristics including the gender and age of the patients were summarized in Table S1. The workflow of the study was shown in Figure 1A. All patients received fluorouracil-based treatment regimens such as XELOX (oxaliplatin, 130 mg/m^2, intravenously, day 1; and capecitabine, 1000 mg/m^2, orally, days 1–14), SOX (oxaliplatin 130 mg/m^2, intravenously, day 1; and S-1, 40–60 mg, twice a day, orally, days 1–14) or DOS (docetaxel 60 mg/m^2, intravenously, day 0; oxaliplatin 130 mg/m^2, intravenously, day 1; and S-1, 40–60 mg, twice a day, orally, days 1–14). Pretreatment serum samples were collected within 14 days before the initiation of preoperative chemotherapies. On-treatment serum samples were collected in day 1 of any on-treatment cycles before infusion of medicines. Post-treatment serum samples were collected after all cycles of preoperative chemotherapy, within 7 days before operations. Peripheral blood samples were collected into a 10 mL EDTA tube before centrifugation for serum samples. Tumor regression was evaluated according to Becker TRG score[57] by at least two experienced pathologists independently. Patients with residual tumor/tumor bed $\leq$50% with chemotherapy effect (Becker TRG score1-2) was regarded as responders. This study was conducted in accordance with the Declaration of Helsinki and was approved by the Institutional Review Board of Zhongshan Hospital of Fudan University. Written consents were obtained from all participants.

METHOD DETAILS

Serum immune proteomics

Proteomic analyses were performed at the laboratory of Sinotech Genomics company (Shanghai, China) without any other information given. The analyses were based on Olink proteomics Target 96 inflammation panel with Proximity Extension Assay (PEA) technology,[58,59] which was based on pairs of antibodies equipped with single-strand oligonucleotide DNA barcodes. Target binding by paired antibodies generated double-stranded DNA amplicons, which could be further quantified to indicate protein levels. Analyses were run with recommended internal control, and inter-plate variability was adjusted by intensity normalization. Protein levels were given as normalized protein expression (NPX) data, which were relative and log2 transformed. A high NPX value corresponded to a high protein concentration. An increase of the NPX value by 1 corresponded to a doubling of the protein level. Target 96 inflammation panel included 92 proteins in important immune and inflammation pathways as listed in Table S4.

PD-1/PD-L1 immunohistochemistry staining

PD-1/PD-L1 immunohistochemistry staining was performed on 4-mm thick formalin-fixed, paraffin-embedded (FFPE) tissue sections. PD-1 was stained with anti-PD-1 (EPR4877(2), Abcam) primary antibody while PD-L1 was stained with anti-PD-L1 (SP142, Abcam primary antibody according to the standard procedures of immunohistochemistry. The intensity and percentage of PD-1/PD-L1 expression in tumor cells and stromal immune cells were evaluated by 2 experienced pathologists independently. PD-L1/PD-1 positivity in stromal/tumor cells was scored as 0, 1, 2, or 3 for <1%, $\geq$1%, but <5%, $\geq$5%, but<10%, or $\geq$10% of cells per area.[12]

Multiplex immunofluorescence

Multiplex immunofluorescence (mIF) was performed on 4-mm thick formalin-fixed, paraffin-embedded (FFPE) tissue sections according to standard procedures. Briefly, tissue sections were stained consecutively with antibodies against the following: FOXP3 (GB112325, Servicebio), CD163(GB14027, Servicebio), CD68(GB113150, Servicebio), CD4 (GB11064, Servicebio) and CD8 (GB12068, Servicebio). The complete stained slides were scanned with the PANNORAMIC MIDI II automatic digital slide scanner system (3dhistech, Hungary). Quantification of cell density (positive cells/mm2 and positive cells/total cells) and colocalization of the biomarkers were performed on completely stained slides using the HALO platform (Indica Labs, USA). Human tonsil FFPE tissues were used with and without primary antibodies as positive and negative (autofluorescence) controls, respectively.

RNA sequencing

Total RNA was extracted from 22 frozen tumor specimens using the RNeasy mini kit (Qiagen, Germany). Paired-end libraries were synthesized using the TruSeqTM RNA Sample Preparation Kit (Illumina, USA) following manufacturer's instructions. Prepared RNA-seq libraries underwent sequencing on the Illumina NovaSeq 6000 (Illumina, USA). Paired-end sequence files (fastq) were mapped to the reference genome (hg 38). Differential genes were calculated by DESeq2 R package.[60] ClusterProfiler R package[61] was used for gene set enrichment analysis (GSEA) of Kyoto Encyclopedia of Genes and Genomes (KEGG) gene sets. Gene sets with both nominal p value and false discovery rate q-value of <0.05 were considered as significantly enriched pathways.

Classic systemic immune-inflammation indices

Results of white blood cell count (WBC), absolute neutrophil count (ANC), absolute lymphocyte count (ALC), absolute monocyte count (AMC), platelet count (PLT), and platelet distribution width (PDW) within 7 days before gastrectomy were extracted from patients' medical records. Indices were calculated using the standard formula: neutrophil to lymphocyte ratio (NLR) = ANC/ALC, platelet to lymphocyte ratio (PLR) = PLT/ALC, monocyte to lymphocyte ratio (MLR) = AMC/ALC.

Consensus clustering and LASSO regression

Unsupervised clustering methods (K-means) for dataset analysis were used to identify pretreatment proteomic patterns and classify patients for further analysis. A consensus clustering algorithm was applied to determine the number of clusters. This procedure was performed using the ConsensuClusterPlus R package[62] and was repeated 1,000 times to ensure the stability of classification. LASSO regression was used to establish pretreatment serum response predictive score (PSRscore) for the prediction of preoperative chemotherapy responses. The glmnet R package[63] was used to perform the LASSO regression model analysis. A λ value = 0.16 with log (λ) = -1.834 was chosen by cross-validation via the 1-SE criteria. The optimal tuning parameter resulted in four non-zero coefficients as indicated in Figure 6F.

QUANTIFICATION AND STATISTICAL ANALYSIS

The normality of the variables was tested by the Shapiro-Wilk normality test. For comparisons of two groups, statistical significance for normally distributed variables was estimated by paired/unpaired student *t* tests, and nonnormally distributed variables were analyzed by Wilcoxon rank-sum test. Correlation coefficients were computed by Spearman or Kendall rank correlation as indicated. The Kaplan–Meier method was used to generate survival curves for the different groups and the log rank test was used to determine statistical significance. The hazard ratios of univariate or multivariate cox proportional hazards regression model were determined by the Survminer R package. The R package pROC was used to plot and visualize receiver operating characteristic (ROC) curves and calculate the area under the curve (AUC) to evaluate the treatment response accuracy of different indices. For all analyses, a two-sided *p* value of <0.05 was considered statistically significant and *p* values were marked as * <0.05, ** <0.01, *** <0.001, **** <0.0001, ***** <0.00001, NS not significant. All data were analyzed using R Statistical Software (version 4.1.0).

Cell Reports Medicine, Volume *4*

Supplemental information

Multiplex immune profiling reveals the role of serum immune proteomics in predicting response to preoperative chemotherapy of gastric cancer

Zhaoqing Tang, Yuan Gu, Zhongyi Shi, Lingqiang Min, Ziwei Zhang, Peng Zhou, Rongkui Luo, Yan Wang, Yuehong Cui, Yihong Sun, and Xuefei Wang

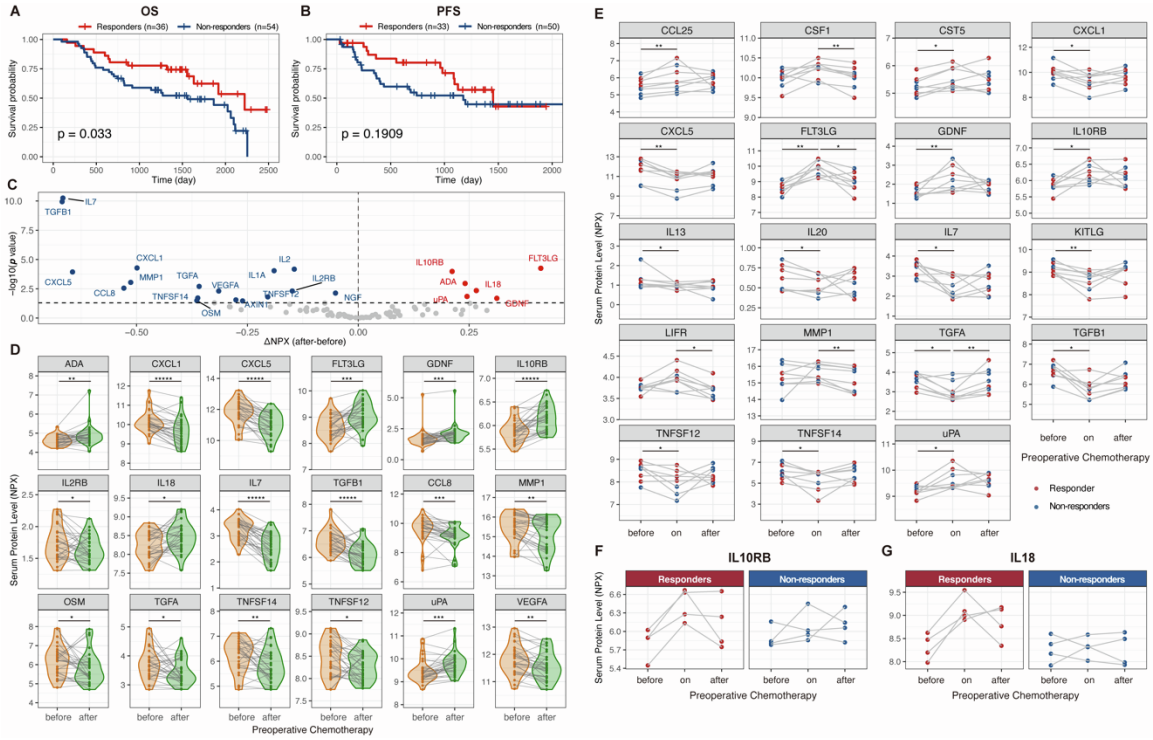

Figure S1. Dynamics of serum immune proteomics during and after preoperative chemotherapy, related to Figure 1. (A). Kaplan–Meier curves of overall survival (OS) for patients with different treatment responses. Log-rank test showed *p*=0.033. (B) Kaplan–Meier curves of progression-free survival (PFS) for patients with different treatment responses. Log-rank test showed *p*=0.1909. (C) Volcano plot showed serum proteins whose levels changed after preoperative chemotherapy in unpaired tests (before n=37, after n=83). (D) The dynamics of the serum proteins showing a significant change after preoperative chemotherapy in both paired and unpaired tests. Only paired serum samples were shown. (E) Dynamics of serum proteins showing a significant change during preoperative chemotherapy. (F) Dynamics of serum IL10RB level during preoperative chemotherapy in responders and non-responders. (G) Dynamics of serum IL18 level during preoperative chemotherapy in responders and non-responders.

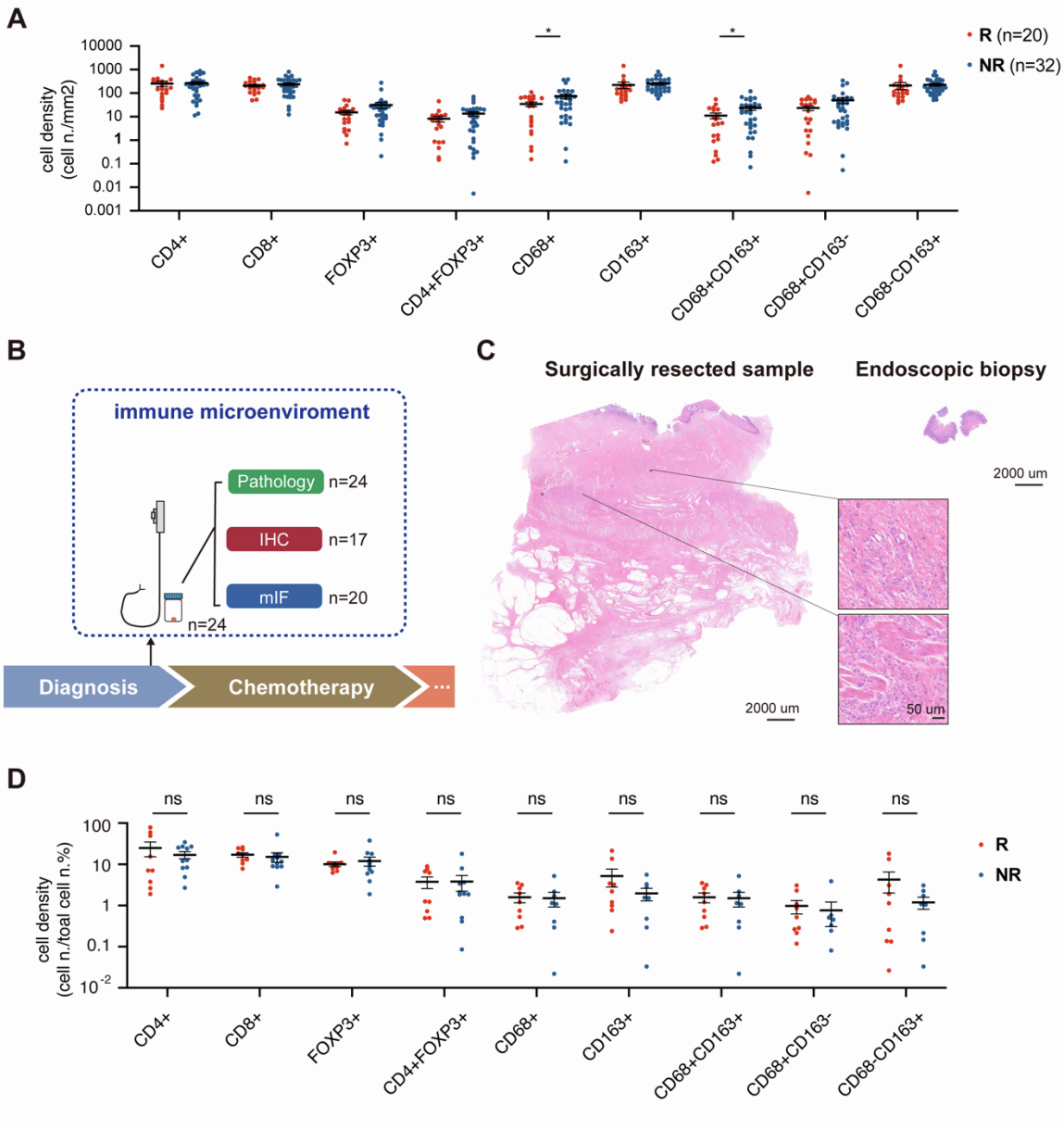

Figure S2. Pretreatment TME features based on endoscopic biopsy, related to Figure 2.

(A) Comparison of immune cell infiltration in post-treatment tumor samples in patients with different treatment responses (responder n=20; non-responder n=32). Cell density calculated by positive cell numbers/area(mm^2). (B) Flow chart of endoscopic biopsy sample collection (C) Representative images of surgically resected samples and endoscopic biopsies. (D) Comparison of immune cell infiltration in pretreatment endoscopic biopsy samples from patients with different treatment responses (responder n=9; non-responder n=11). Cell density calculated by positive cell numbers/total cell numbers.

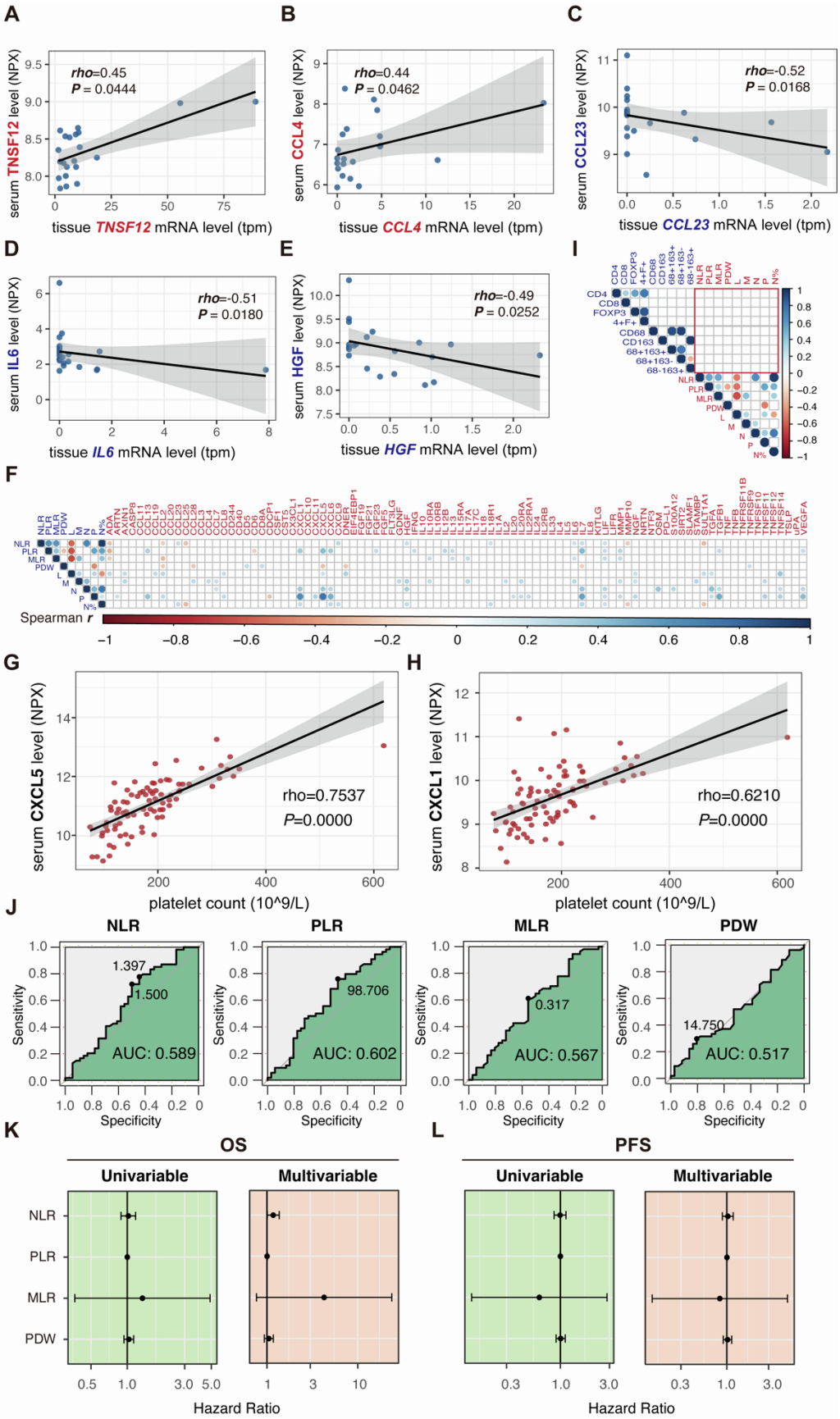
A
serum TNSF12 level (NPX)
rho=0.45
P = 0.0444
tissue TNSF12 mRNA level (tpm)
B
serum CCL4 level (NPX)
rho=0.44
P = 0.0462
tissue CCL4 mRNA level (tpm)
C
serum CCL23 level (NPX)
rho=-0.52
P = 0.0168
tissue CCL23 mRNA level (tpm)
D
serum IL6 level (NPX)
rho=-0.51
P = 0.0180
tissue IL6 mRNA level (tpm)
E
serum HGF level (NPX)
rho=-0.49
P = 0.0252
tissue HGF mRNA level (tpm)
I
F
Spearman r
G
serum CXCL5 level (NPX)
rho=0.7537
P=0.0000
platelet count (10^9/L)
H
serum CXCL1 level (NPX)
rho=0.6210
P=0.0000
platelet count (10^9/L)
J
NLR
PLR
MLR
PDW
Sensitivity
Specificity
1.397
1.500
AUC: 0.589
98.706
AUC: 0.602
0.317
AUC: 0.567
14.750
AUC: 0.517
K
OS
Univariable
Multivariable
NLR
PLR
MLR
PDW
Hazard Ratio
L
PFS
Univariable
Multivariable
Hazard Ratio

Figure S3. Correlations between local and systemic immune features and clinical value of classic systemic immune-inflammation indices, related to Figure 3. (A) Correlation between post-treatment serum TNSF12 level and tissue *TNF12* mRNA level. (B) Correlation between post-treatment serum CCL4 level and tissue *CCL4* mRNA level. (C) Correlation between post-treatment serum CCL23 level and tissue *CCL23* mRNA level. (D) Correlation between post-treatment serum IL6 level and tissue *IL6* mRNA level. (E) Correlation between post-treatment serum HGF level and tissue *HGF* mRNA level. The *rho* values and *p* values of Spearman's correlation were indicated. (F) Correlations between post-treatment serum proteomics and four immune-inflammation indices, and common blood cell counts. *Rho* values of correlations with *p* value<0.05 were indicated by different colors as indicated (G) Correlation between post-treatment serum CXCL5 level and peripheral blood platelet count. (H) Correlation between post-treatment serum CXCL1 level and peripheral blood platelet count. *Rho* and *p* values of Spearman correlation as indicated. (I) Correlations between classic systemic immune-inflammation indices and immune cell infiltration in TME. The rho values of correlations with *p* value<0.05 were indicated by different colors as indicated. (J) ROC curve demonstrating treatment response predictive accuracy of four classic systemic immune-inflammation indices. (K) Hazard ratio (HR) of four classic systemic immune-inflammation indices for overall survival (OS) calculated by univariable/multivariable cox regression. (L) Hazard ratio (HR) of four classic systemic immune-inflammation indices for progression-free survival (PFS) calculated by univariable/ multivariable cox regression.

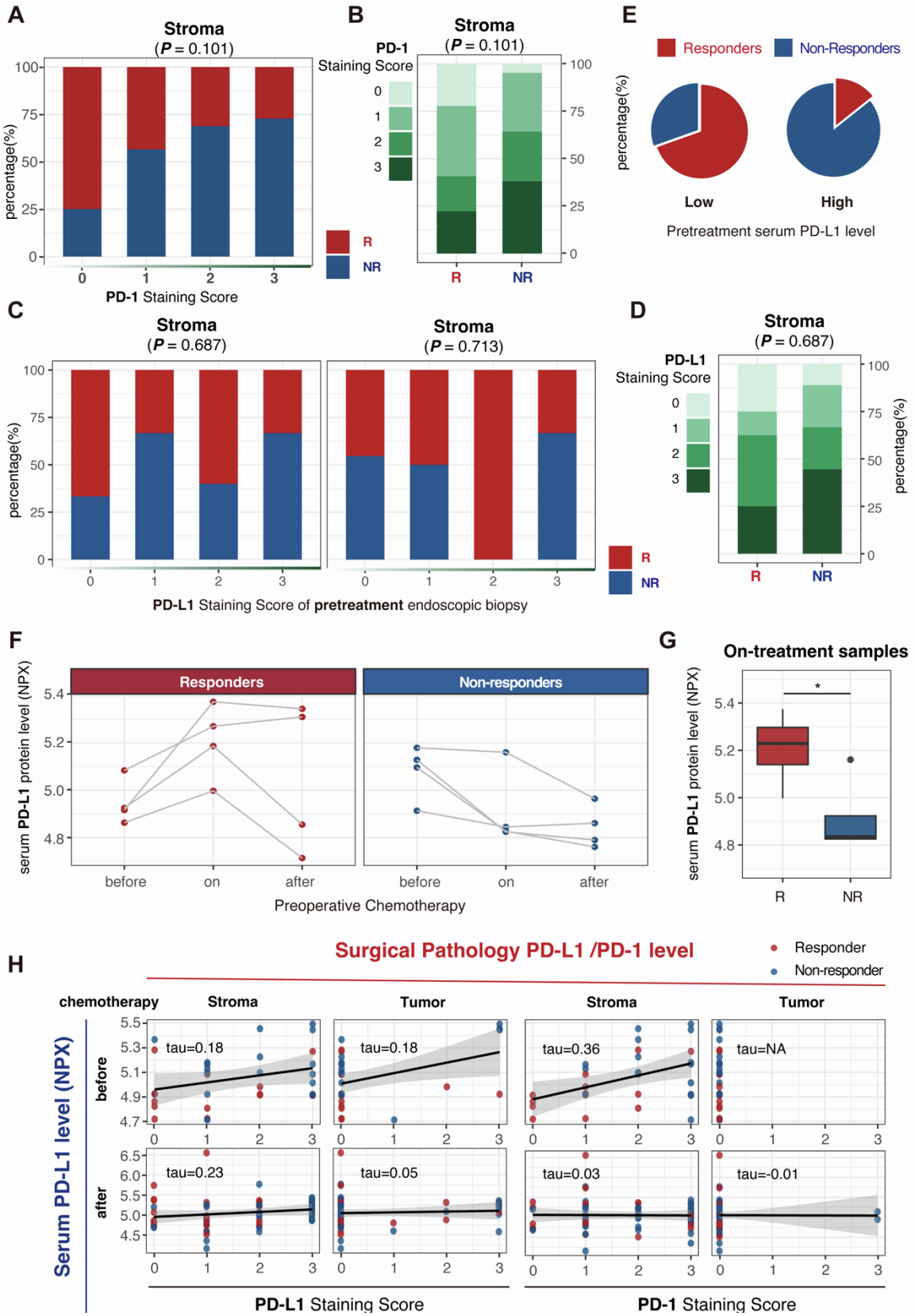

Figure S4. Correlation between tissue PD1/PD-L1 staining and serum PD-L1 level, and their

associations with treatment response, related to Figure 4. (A) Treatment response in patients (n=70) with different stromal PD-1 staining scores. (B) Stromal PD-1 staining scores in patients with different treatment response (responders n=33, non-responders n=50). (C) Treatment response in patients (n=17) with different stromal/tumor PD-L1 staining scores of their pretreatment endoscopic biopsies. (D) Pretreatment stromal PD-L1 staining scores of patients with different treatment responses. (E) Treatment responses in patients with high (>5.084 NPX, n=14) and low (<5.084 NPX, n=23) pretreatment serum PD-L1 level. (F) Dynamics of serum PD-L1 level during preoperative chemotherapy. (G) On-treatment serum PD-L1 level differed in patients with different responses. (H) Correlation between surgical pathology PD-L1 /PD-1 level and serum PD-L1 level. *Tau* values of Kendall rank correlation were indicated.

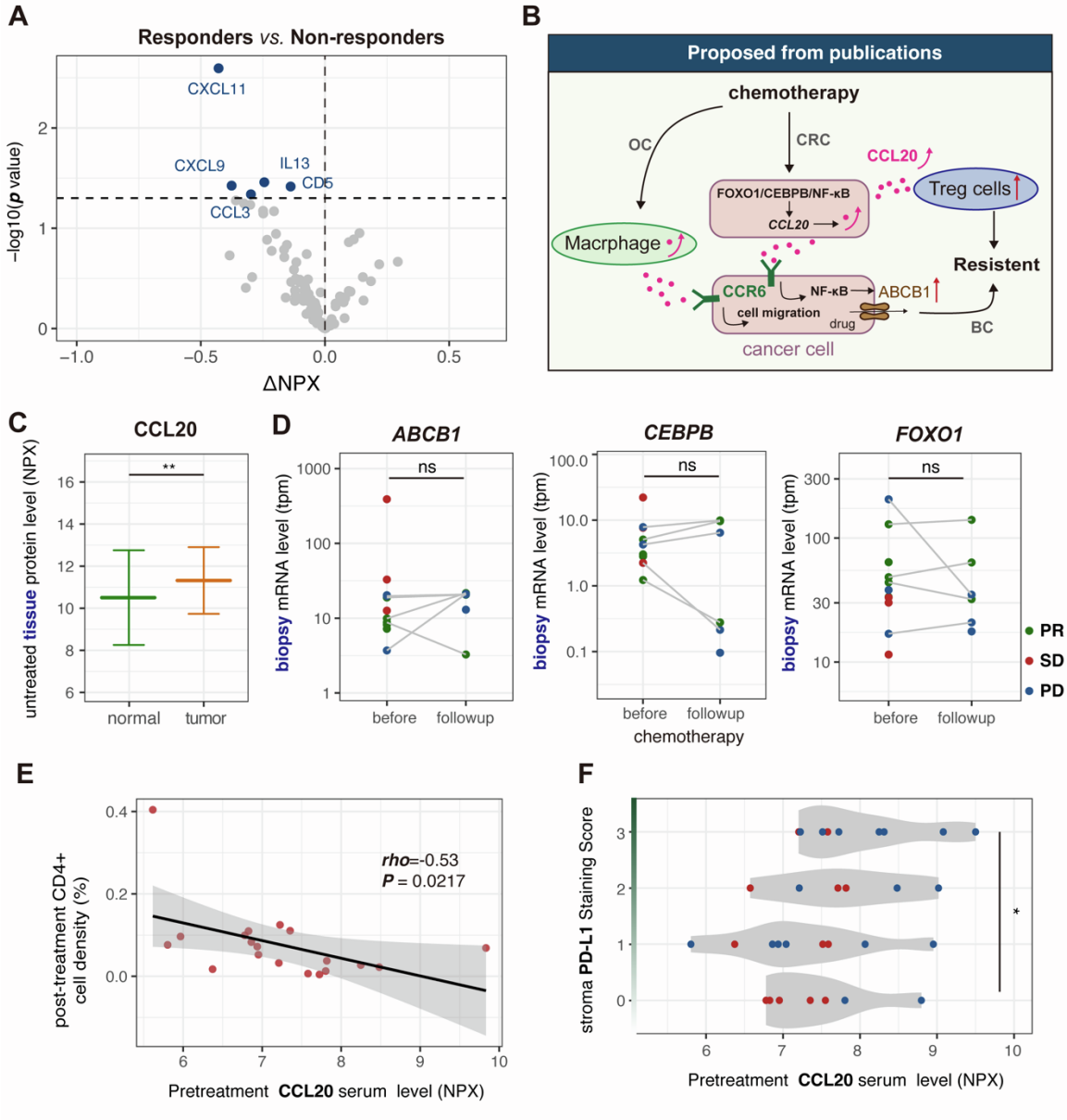

Figure S5. Potential role of CCL20 in chemoresistance, related to Figure 5. (A) Comparison of post-treatment serum protein levels in responders and non-responders. (B) Mechanisms of *CCL20* upregulation reported in breast cancer (BC), ovarian cancer (OC), and colorectal cancer (CRC). (C) Gastric tumor had higher CCL20 protein level compared with normal gastric tissues. (D) Biopsy tumor sample showed no change in *ABCB*, *CEBPB*, and *FOXO1* mRNA level before and during treatment in patients with gastric cancer undergoing first-line standard chemotherapy. (E) Higher pretreatment CCL20 level was linked to less CD4(+) T cell infiltration in post-treatment tumors. (F) Higher pretreatment CCL20 level was linked to higher stromal PD-L1 staining in post-treatment tumors.

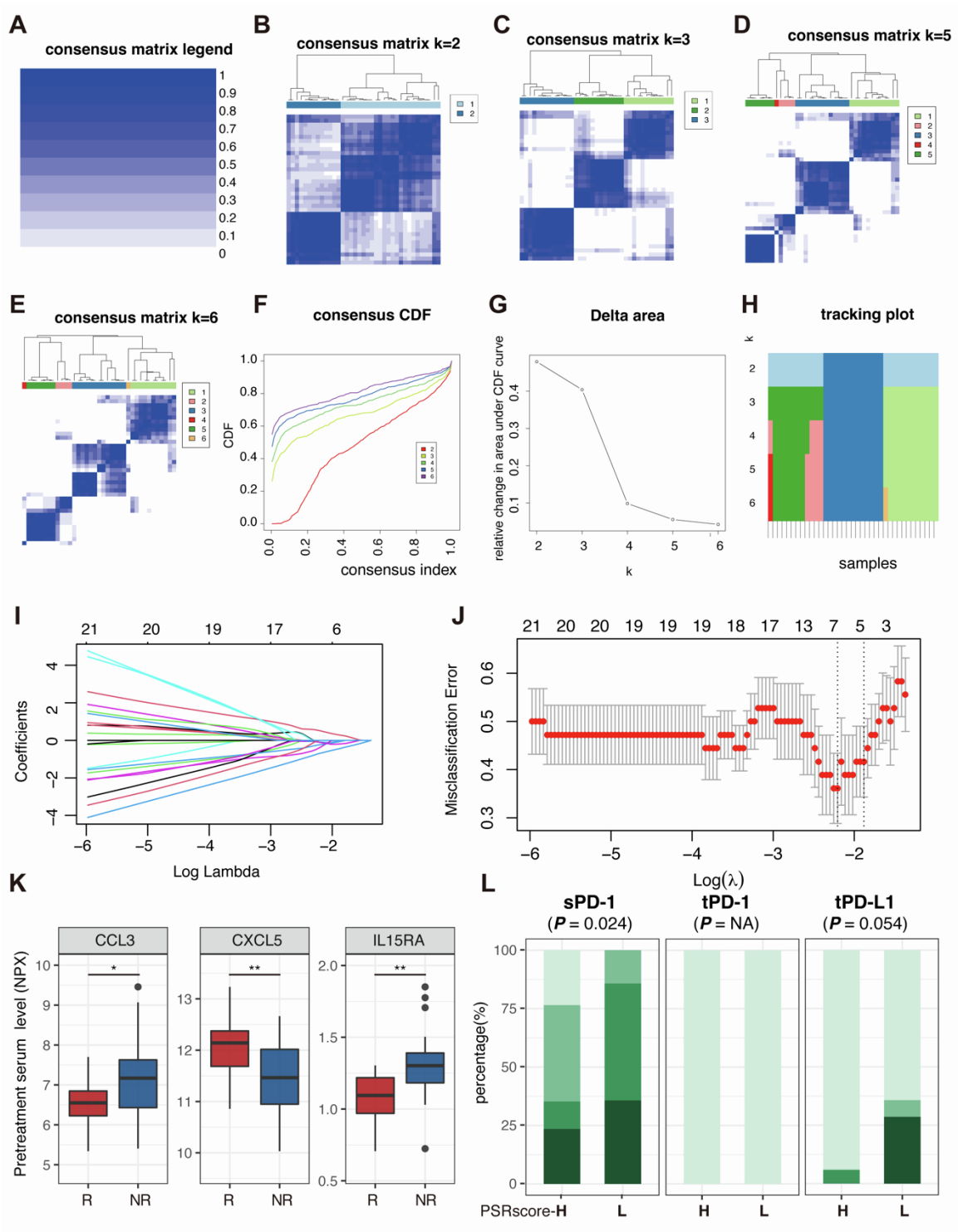

Figure S6. Unsupervised consensus clustering and LASSO model of pretreatment serum proteomics, related to Figure 6. (A -E) Consensus matrix heat maps based on the number of clusters (from k=2 to 6). (F) Cumulative distribution function (CDF) under corresponding k values. (G) Relative change in area (delta area) under the cumulative distribution function (CDF) curves when the cluster number varies from k=2 to 6. (H) Sample clustering under different k values. (I) Average error and standard deviation over the folds after

k-fold cross-validation in LASSO model. (J) Misclassification error in different λ value. A λ value= 0.16 with log (λ) = -1.834 was chosen by cross-validation via the 1-SE criteria. (K) Responders (n=18) had lower serum CCL3 and IL15RA level and higher CXCL5 level before chemotherapy compared with non-responders (n=19). (L) Post-treatment stromal PD-1 level and tumor PD-1/PD-L1 level in patients with high/low PSRscores (H: n=18, L: n=14).

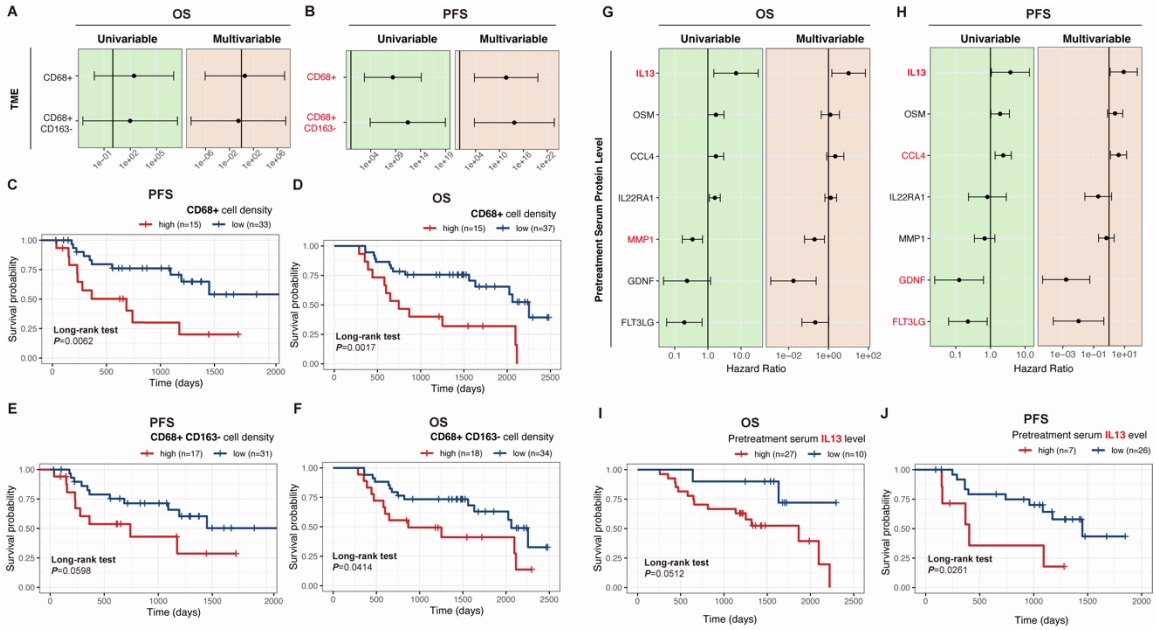

Figure S7. Prognostic value of immune cell infiltration in TME and pretreatment serum proteomics, related to Figure 7. (A) Hazard ratios (HR) of different immune cell infiltration in TME for overall survival calculated by univariable/ multivariable cox regression. (B) HR of different immune cell infiltration in TME for progression-free survival calculated by univariable/ multivariable cox regression. The length of the horizontal line represented the 95% confidence interval of HR for each protein. The vertical solid line represented HR= 1. (C) Kaplan–Meier curves of PFS for patients with high (n=15) and low (n=33) CD68(+) cell infiltration. (D) Kaplan–Meier curves of OS for patients with high (n=15) and low (n=37) CD68(+) cell infiltration. (E) Kaplan–Meier curves of PFS for patients with high (n=17) and low (n=31) CD68(+) and CD163(-) cell infiltration. (F) Kaplan–Meier curves of OS for patients with high (n=18) and low (n=34) CD68(+) and CD163(-) cell infiltration. The *p* value of Log-rank test and HR of multivariable cox regression were indicated. (G) Hazard ratios (HR) of pretreatment serum protein levels for overall survival calculated by univariable/ multivariable cox regression. (H) HR of post-treatment serum protein levels for progression-free survival calculated by univariable/ multivariable cox regression. The length of the horizontal line represented the 95% confidence interval of HR for each protein. The vertical solid line represented HR= 1. (I) Kaplan–Meier curves of overall survival (OS) for patients with high (n=27) and low (n=10) post-treatment serum IL13 level. (J) Kaplan–Meier curves of progression-free survival (PFS) for patients with high (n=7) and low (n=26) post-treatment serum IL13 level. The *p* value of Log-rank test and HR of multivariable cox regression were indicated.

Tables

Table S1. Clinical characteristics of patients, related to Figure 7.

Response	Good	Poor	Total	*P* value
N	36	54	90	
gender = M (%)	26 (72.2)	42 (77.8)	68 (75.6)	0.726
age = >=60 (%)	19 (52.8)	32 (59.3)	51 (56.7)	0.696
location = non-AEJ (%)	31 (86.1)	39 (72.2)	70 (77.8)	0.196
Lauren (%)				0.846
diffuse	9 (25.0)	14 (25.9)	23 (25.6)	
Intestinal	15 (41.7)	25 (46.3)	40 (44.4)	
mixed	12 (33.3)	15 (27.8)	27 (30.0)	
differentiation (%)				0.083
G2	11 (30.6)	8 (14.8)	19 (21.1)	
G3	24 (66.7)	46 (85.2)	70 (77.8)	
Gx	1 (2.8)	0 (0.0)	1 (1.1)	
regimens (%)				0.167
Two-drug	14 (38.9)	29 (53.7)	43 (47.8)	
Three-drug	21 (58.3)	21 (38.9)	42 (46.7)	
Other	1 (2.8)	4 (7.4)	5 (5.6)	
ypT (%)				0.312
1a	2 (5.6)	1 (1.9)	3 (3.3)	
1b	3 (8.3)	1 (1.9)	4 (4.4)	
2	10 (27.8)	12 (22.2)	22 (24.4)	
3	11 (30.6)	20 (37.0)	31 (34.4)	
4a	9 (25.0)	20 (37.0)	29 (32.2)	
X	1 (2.8)	0 (0.0)	1 (1.1)	
ypN (%)				<0.001
0	19 (52.8)	8 (14.8)	27 (30.0)	
1	11 (30.6)	10 (18.5)	21 (23.3)	
2	0 (0.0)	15 (27.8)	15 (16.7)	
3a	6 (16.7)	9 (16.7)	15 (16.7)	
3b	0 (0.0)	12 (22.2)	12 (13.3)	
ypM = 1 (%)	13 (36.1)	13 (24.1)	26 (28.9)	0.319
ypTNM (%)				0.021
I	9 (25.0)	5 (9.3)	14 (15.6)	
II	7 (19.4)	11 (20.4)	18 (20.0)	
III	6 (16.7)	25 (46.3)	31 (34.4)	
IV	13 (36.1)	13 (24.1)	26 (28.9)	
Other	1 (2.8)	0 (0.0)	1 (1.1)	
LVI = Positive (%)	10 (27.8)	31 (57.4)	41 (45.6)	0.011

PNI = Positive (%)	18 (50.0)	35 (64.8)	53 (58.9)	0.238

Table S2. Multivariate survival analysis of serum post-treatment IL10RB level based on OS, related to Figure 7.

	univariable cox regression			multivariable cox regression		
Characteristics	**Hazard ratio (95% CI)**	***P* value**		**Hazard ratio (95% CI)**	***P* value**	
gender = M	0.7146 (0.3791, 1.347)	0.299		1.407 (0.5225, 3.769)	0.497	
age = >=60	0.704 (0.3885, 1.276)	0.247		0.5613 (0.2468, 1.277)	0.168	
location= non-AEJ	1.671 (0.7454, 3.745)	0.213				
Lauren						
diffuse	reference			Reference		
Intestinal	0.3014 (0.1458, 0.6232)	0.001	**	0.4279 (0.1498, 1.222)	0.113	
mixed	0.5435 (0.2708, 1.0909)	0.086	.	0.6309 (0.2337, 1.703)	0.363	
differentiation						
G2	reference			Reference		
G3	4.438 (1.3675, 14.4)	0.013	*	1.54 (0.3791, 6.259)	0.546	
Gx	6.936 (0.7154, 67.24)	0.095	.	1.385 (0.1084, 17.697)	0.802	
regimens (%)						
Other	reference					
Two-drug	1.232 (0.3591, 4.227)	0.740				
Three-drug	1.536 (0.4475, 5.272)	0.495				
ypTNM						
I	reference			Reference		
II	2.522 (0.5074, 12.54)	0.258		3.053 (0.3335, 27.95)	0.323	
III	6.08 (1.4182, 26.07)	0.015	*	5.332 (0.6065, 46.873)	0.131	
IV	6.259 (1.4427, 27.15)	0.014	*	10.08 (1.2552, 80.883)	0.030	*
Other	0 (0, Inf)	0.997		0 (0, Inf)	0.998	
LVI = Positive	2.867 (1.524, 5.391)	0.001	**	1.996 (0.9191, 4.334)	0.081	.
PNI = Positive	2.033 (1.062, 3.892)	0.032	*	1.431 (0.6281, 3.262)	0.393	
IL10RB level	3.086 (1.055, 9.031)	0.040	*	5.622 (1.7884, 17.676)	0.003	**

Table S3. Multivariable cox regression of post-treatment serum IL10RB level based on PFS, related to Figure 7.

	univariable cox regression			multivariable cox regression		
Characteristics	**Hazard ratio (95% CI)**	***P* value**		**Hazard ratio (95% CI)**	***P* value**	
gender = M	0.8883 (0.4025, 1.961)	0.769		1.109 (0.3878,3.173)	0.846	
age = >=60	0.7027 (0.3619,1.364)	0.297		0.491 (0.2101,1.147)	0.100	
location= non-AEJ	1.507 (0.5844,3.884)	0.396				
Lauren						
diffuse	reference			reference		
Intestinal	0.3920 (0.1725,0.8907)	0.0253	*	0.8374 (0.2711,2.587)	0.758	
mixed	0.8524 (0.3821,1.9015)	0.6964		1.484 (0.4185,5.261)	0.541	
differentiation						
G2	reference					
G3	2.2569 (0.8714,5.846)	0.0937	.			
Gx	3.104 (0.3609,26.693)	0.3022				
regimens (%)						
other	reference					
Two-drug	1.483 (0.1980,11.1)	0.701				
Three-drug	1.369 (0.1803,10.39)	0.761				
ypTNM						
I	reference			reference		
II	1.290 (0.3634,4.581)	0.693		1.702 (0.3868,7.489)	0.482	
III	2.402 (0.7942,7.267)	0.121		3.566 (0.7414,17.152)	0.113	
IV	2.211 (0.6925,7.06)	0.180		4.816 (1.1227,20.654)	0.034	*
other	0 (0,Inf)	0.997		0 (0,Inf)	0.997	
LVI = Positive	1.978 (1.008 ,3.884)	0.0474	*	1.529 (0.61,3.832)	0.365	
PNI = Positive	2.782 (1.262,6.135)	0.0112	*	3.464 (1.2484,9.61)	0.017	*
IL10RB level	4.3918 (1.185,16.27)	0.0268	*	14.35 (3.0624,67.216)	0.001	***

Table S4. Proteins included in Olink proteomics Target 96 inflammation panel, related to serum immune proteomics in STAR Methods.

UniprotID	Protein name	abbrevation
O00300	Osteoprotegerin (OPG)	TNFRSF1 1B
O14625	C-X-C motif chemokine 11 (CXCL11)	CXCL11
O14788	TNF-related activation-induced cytokine (TRANCE)	TNFSF11
O15169	Axin-1 (AXIN1)	AXIN1
O15444	C-C motif chemokine 25 (CCL25)	CCL25
O43508	Tumor necrosis factor (Ligand) superfamily, member 12 (TWEAK)	TNFSF12
O43557	Tumor necrosis factor ligand superfamily member 14 (TNFSF14)	TNFSF14
O95630	STAM-binding protein (STAMPB)	STAMBP
O95750	Fibroblast growth factor 19 (FGF-19)	FGF19
O95760	Interleukin-33 (IL-33)	IL33
P00749	Urokinase-type plasminogen activator (uPA)	uPA
P00813	Adenosine Deaminase (ADA)	ADA
P01135	Transforming growth factor alpha (TGF-alpha)	TGFA
P01137	Latency-associated peptide transforming growth factor beta-1 (LAP TGF-beta-1)	TGFB1
P01138	Beta-nerve growth factor (Beta-NGF)	NGF
P01374	TNF-beta (TNFB)	TNFB
P01375	Tumor necrosis factor (TNF)	TNF
P01579	Interferon gamma (IFN-gamma)	IFNG
P01583	Interleukin-1 alpha (IL-1 alpha)	IL1A
P01732	T-cell surface glycoprotein CD8 alpha chain (CD8A)	CD8A
P02778	C-X-C motif chemokine 10 (CXCL10)	CXCL10
P03956	Matrix metalloproteinase-1 (MMP-1)	MMP1
P05112	Interleukin-4 (IL-4)	IL4
P05113	Interleukin-5 (IL5)	IL5
P05231	Interleukin-6 (IL6)	IL6
P06127	T-cell surface glycoprotein CD5 (CD5)	CD5
P09238	Matrix metalloproteinase-10 (MMP-10)	MMP10
P09341	C-X-C motif chemokine 1 (CXCL1)	CXCL1
P09603	Macrophage colony-stimulating factor 1 (CSF-1)	CSF1
P10145	Interleukin-8 (IL-8)	IL8
P10147	C-C motif chemokine 3 (CCL3)	CCL3
P12034	Fibroblast growth factor 5 (FGF-5)	FGF5
P13232	Interleukin-7 (IL-7)	IL7
P13236	C-C motif chemokine 4 (CCL4)	CCL4
P13500	Monocyte chemotactic protein 1 (MCP-1)	CCL2
P13725	Oncostatin-M (OSM)	OSM
P14210	Hepatocyte growth factor (HGF)	HGF
P14784	Interleukin-2 receptor subunit beta (IL-2RB)	IL2RB

P15018	Leukemia inhibitory factor (LIF)	LIF
P15692	Vascular endothelial growth factor A (VEGF-A)	VEGFA
P20783	Neurotrophin-3 (NT-3)	NTF3
P21583	Stem cell factor (SCF)	KITLG
P22301	Interleukin-10 (IL10)	IL10
P25942	CD40L receptor (CD40)	CD40
P28325	Cystatin D (CST5)	CST5
P29460	Interleukin-12 subunit beta (IL-12B)	IL12B
P30203	T cell surface glycoprotein CD6 isoform (CD6)	CD6
P35225	Interleukin-13 (IL-13)	IL13
P39905	Glial cell line-derived neurotrophic factor (GDNF)	GDNF
P42702	Leukemia inhibitory factor receptor (LIF-R)	LIFR
P42830	C-X-C motif chemokine 5 (CXCL5)	CXCL5
P49771	Fms-related tyrosine kinase 3 ligand (Flt3L)	FLT3LG
P50225	Sulfotransferase 1A1 (ST1A1)	SULT1A1
P50591	TNF-related apoptosis-inducing ligand (TRAIL)	TNFSF10
P51671	Eotaxin (CCL11)	CCL11
P55773	C-C motif chemokine 23 (CCL23)	CCL23
P60568	Interleukin-2 (IL-2)	IL2
P78423	Fractalkine (CX3CL1)	CX3CL1
P78556	C-C motif chemokine 20 (CCL20)	CCL20
P80075	Monocyte chemotactic protein 2 (MCP-2)	CCL8
P80098	Monocyte chemotactic protein 3 (MCP-3)	CCL7
P80162	C-X-C motif chemokine 6 (CXCL6)	CXCL6
P80511	Protein S100-A12 (EN-RAGE)	S100A12
Q07011	Tumor necrosis factor receptor superfamily member 9 (TNFRSF9)	TNFRSF9
Q07325	C-X-C motif chemokine 9 (CXCL9)	CXCL9
Q08334	Interleukin-10 receptor subunit beta (IL-10RB)	IL10RB
Q13007	Interleukin-24 (IL-24)	IL24
Q13261	Interleukin-15 receptor subunit alpha (IL-15RA)	IL15RA
Q13291	Signaling lymphocytic activation molecule (SLAMF1)	SLAMF1
Q13478	Interleukin-18 receptor 1 (IL-18R1)	IL18R1
Q13541	Eukaryotic translation initiation factor 4E-binding protein 1 (4E-BP1)	EIF4EBP1
Q13651	Interleukin-10 receptor subunit alpha (IL-10RA)	IL10RA
Q14116	Interleukin-18 (IL-18)	IL18
Q14790	Caspase-8 (CASP-8)	CASP8
Q16552	Interleukin-17A (IL-17A)	IL17A
Q5T4W7	Artemin (ARTN)	ARTN
Q8IXJ6	SIR2-like protein 2 (SIRT2)	SIRT2
Q8N6P7	Interleukin-22 receptor subunit alpha-1 (IL-22 RA1)	IL22RA1
Q8NFT8	Delta and Notch-like epidermal growth factor-related receptor (DNER)	DNER

Q969D9	Thymic stromal lymphopoietin (TSLP)	TSLP
Q99616	Monocyte chemotactic protein 4 (MCP-4)	CCL13
Q99731	C-C motif chemokine 19 (CCL19)	CCL19
Q99748	Neurturin (NRTN)	NRTN
Q9BZW8	Natural killer cell receptor 2B4 (CD244)	CD244
Q9GZV9	Fibroblast growth factor 23 (FGF-23)	FGF23
Q9H5V8	CUB domain-containing protein 1 (CDCP1)	CDCP1
Q9NRJ3	C-C motif chemokine 28 (CCL28)	CCL28
Q9NSA1	Fibroblast growth factor 21 (FGF-21)	FGF21
Q9NYY1	Interleukin-20 (IL-20)	IL20
Q9NZQ7	Programmed cell death 1 ligand 1 (PD-L1)	PD-L1
Q9P0M4	Interleukin-17C (IL-17C)	IL17C
Q9UHF4	Interleukin-20 receptor subunit alpha (IL-20RA)	IL20RA